

promoting access to White Rose research papers



Universities of Leeds, Sheffield and York
<http://eprints.whiterose.ac.uk/>

This is an author produced version of a paper published in **Surveys in Geophysics**

White Rose Research Online URL for this paper:

<http://eprints.whiterose.ac.uk/id/eprint/77377>

Paper:

Angus, DAC (2013) *The one-way wave equation: a full-waveform tool for modeling seismic body wave phenomena*. Surveys in Geophysics

<http://dx.doi.org/10.1007/s10712-013-9250-2>

The one-way wave equation: a full-waveform tool for modeling seismic body wave phenomena

D.A. Angus

School of Earth & Environment, University of Leeds, d.angus@leeds.ac.uk

2 July 2013

Abstract

The study of seismic body waves is an integral aspect in global, exploration and engineering scale seismology, where the forward modeling of waves is an essential component in seismic interpretation. Forward modeling represents the kernel of both migration and inversion algorithms as the Green's function for wavefield propagation, and is also an important diagnostic tool that provides insight into the physics of wave propagation and a means of testing hypotheses inferred from observational data. This paper introduces the one-way wave equation method for modeling seismic wave phenomena and specifically focuses on the so-called operator-root one-way wave equations. To provide some motivation for this approach, this review first summarizes the various approaches in deriving one-way approximations and subsequently discusses several alternative matrix narrow-angle and wide-angle formulations. To demonstrate the key strengths of the one-way approach, results from waveform simulation for global scale shear-wave splitting modeling, reservoir-scale frequency dependent shear-wave splitting modeling, and acoustic waveform modeling in random heterogeneous media are shown. These results highlight the main feature of the one-way wave equation approach in terms of its ability to model gradual vector (for the elastic case) and scalar (for the acoustic case) waveform evolution along the underlying wavefront. Although not strictly an exact solution, the one-way wave equation shows significant advantages (e.g., computational efficiency) for a range of transmitted wave three-dimensional global, exploration and engineering scale applications.

1 Introduction

The analysis of seismic waves is a key component in global Earth studies, hydrocarbon exploration and, more recently, mineral exploration and engineering scale applications. Seismic waves provide a means of remotely sensing the Earth's subsurface with resolvable scales on the order of hundreds of kilometres to less than a meter. Interpretation of recorded seismic waves, whether they be

from earthquakes or controlled-sources, frequently involves producing a ‘seismic image’. Most often this image takes the form of some parameter distribution (e.g., velocity and density) or some geometric representation (e.g., structural and stratigraphic interfaces).

The seismic image is obtained through migration or inversion of seismic data. Forward modeling of waves is an essential component in both migration and inversion algorithms which require either the reverse propagation (i.e., downward continuation) of the observed seismic data or the forward propagation of synthetic seismic data. Forward modeling is also an important diagnostic tool that provides insight into the physics of wave propagation and a means of testing hypotheses inferred from observational data. Since there is no general analytic solution to the elastic wave equation for anisotropic, inhomogeneous media, various approximate methods are used and these are often based on physically-motivated arguments specific to the problem under study [see 1, for a review].

In [1] the authors classify and summarize forward modeling into three general categories: full-wave equation methods, integral-equation methods and ray-based methods. However, it is often difficult to draw a clear distinction, as many of the various approaches overlap in subtle ways. For most problems, there is generally no one ‘correct’ approach, but rather a range of acceptable approaches that can be used to evaluate the solution. For instance, if direct arrivals are of interest, where the first-order effects of material averaging (or wavelength smoothing) can be modeled by a gradually varying medium and the wave path lengths are not too great, then basic ray methods or more advanced ray-coupling approaches should be applicable. On the other hand, if strong multiple scattering and/or wide-angle diffraction is important, a numerical solution of the full anisotropic elastic wave equation is necessary. Thus, selecting an appropriate method involves weighing the advantages and disadvantages of all acceptable approaches in terms of accuracy requirements and computational limitations.

Finite-difference/finite-element and basic geometrical-ray methods are essentially end member approaches to wave simulation. Finite-difference [e.g., 2; 3], finite-element [e.g., 4; 5] or pseudo-spectral methods [e.g., 6; 7] applied to the full-wave equation will correctly predict all physical signals. However, these methods can be costly in terms of computing requirements and the complete synthetic seismograms may not actually be necessary. Basic geometrical-ray theory [e.g., 8] is more intuitive and computationally less expensive, but neglects often important effects. Between these end members are the so-called hybrid methods. Extensions to basic ray theory are the Kirchhoff [e.g., 9; 10], Maslov [e.g., 11; 12], Gaussian beam [e.g., 13] and coherent-state [e.g., 14] methods, which describe additional diffraction effects to various degrees. Transform methods involve separating the partial differential wave equation into an ordinary differential wave equation with appropriate boundary conditions [see 11, for a review] and are suitable for homogeneous [e.g., 15] and weakly heterogeneous [e.g., 11] layered media. For finite heterogeneities, the interaction of wavefield with scatterers often tends to be difficult to evaluate with ray-based

methods. For these cases the scattered or diffracted wavefield can be considered as secondary seismic sources, and hence are often modeled using the Born [e.g., 16; 17; 18; 19] or Rytov [e.g., 20; 21] approximations. The Born and Rytov approximations are similar in that they both assume weak scattering. However, the Rytov approximation differs from the Born approximation in that the phase relation of the incident and scattered wavefield is linear, rather than the amplitude. Although computationally impractical, the path-integral approach [e.g., 22; 23] is conceptually attractive because it provides a link between many of the ray-based methods and the full-wave equation methods. Variations on the finite-difference approach are the one-way [e.g., 24; 25; 26] and the phase-screen [e.g., 27; 28; 29; 30] methods. These approaches are intended to reduce the computational costs while retaining some of the more important wave effects, but generally neglect backscatter. The following discussion intends to briefly touch upon the major ideas behind and the motivation for using the one-way wave equation technique in seismology [for applications in other fields refer to 20; 31; 32].

The one-way or parabolic wave equation technique was first introduced by [33] and applied to the problem of atmospheric radio wave propagation [see 32]. It has subsequently been used extensively in many wave propagation studies spanning several branches of physics (e.g., optics, electro-magnetics, underwater acoustics and seismology). Interestingly, the field of ocean acoustics has had a significant influence on the initial seismic research [see 31] and this is perhaps attributable to the fact that both communities were focusing on practical applications of the acoustic wave equation. Applications of one-way wave equations in seismology have been as wavefield propagators in studying reflection problems [e.g., 24] or as Green's functions (e.g., in evaluating the wavefield of Gaussian beams). Parabolic wave equations have also been used for practical purposes as absorbing boundary conditions in full-wave equation finite-difference (FD) methods [e.g., 34].

The derivations of the parabolic wave equation can be split into two categories: methods that factorize the wave solution [e.g., 24] and methods that factorize the wave equation [e.g., 35]. In both cases, factorization involves choosing a preferred axis or direction of propagation and splitting the solution or differential operator into two factors, one factor representing forward-travelling waves and the other factor reverse-travelling waves. This factorization reduces the second-order wave equation into two first-order equations. This reduction to first-order with respect to a preferred axis limits one-way wave equations to transmission problems, since backscatter is neglected, but allows a decrease of several orders of magnitude in computational effort. Further approximations or simplifications tend to improve the computational efficiency of these approaches, but at the expense of accurately representing the 'true' one-way wavefield.

This paper introduces the one-way wave equation method for modeling seismic wave phenomena and specifically focuses on the one-way elastic wave equation derived by [36] and implemented by [37; 38; 39; 40]. I first discuss the 3×3 matrix formulation of [36], starting with the exact operator for homogeneous media, then approximate operator for inhomogeneous media, and finally the

narrow-angle approximations. I also review the acoustic wide-angle formulation of [41] and implementation by [42]. I show results of waveform simulation for global scale shear-wave splitting (SWS) modeling, reservoir-scale frequency dependent shear-wave splitting modeling, and acoustic waveform modeling in random heterogeneous media.

2 Brief history of parabolic and one-way wave equations

The parabolic approximation was first introduced to ocean acoustics to solve transmission problems by reducing the two-dimensional (2D) acoustic wave equation [see 25; 31]. This approximation to the acoustic wave equation was applied to seismological problems by [24] and [43] and subsequently extended to reduce the 2D elastic wave equation by [44], [34] and [45]. These one-way wave equations are commonly referred to as 15° approximations because they are judged accurate for propagation angles up to about 15° from the preferred direction of propagation [46]. Since one-way wave equations are in fact expressions for the first spatial derivative of a wavefield (i.e., the first derivative with respect to the preferred direction) they are also referred to as wave extrapolation equations or wave extrapolators [46]. That is, given an initial wavefield and its derivative, that wavefield can be extrapolated or propagated using a variety of numerical means. This type of wavefield extrapolation has been found particularly useful in the migration of seismic data [47].

The above parabolic approximations are commonly referred to as ‘reference phase’ approaches. This is because they involve extracting a reference phase from the wave solution in the process of simplifying the wave equation. The wave solution consists of an oscillatory phase component and a slowly varying amplitude component. By extracting the reference phase $\exp[i(\omega/c_0)x_1]$, where ω is frequency, x_1 is the preferred direction of propagation and c_0 is a reference velocity, the oscillatory component can be reduced, leaving only the slowly varying amplitude component. Since this amplitude term is slowly varying, various spatial derivatives can be omitted by making certain assumptions about the wavefield (e.g., near plane-wave propagation) and the medium (e.g., weak heterogeneity). Applying the reference phase approach to the 2D acoustic wave equation yields the so-called 15° parabolic wave equation

$$\partial_1 u^+ = \frac{i}{2k} (\partial_2^2 + \epsilon k^2) u^+ \quad (1)$$

[24, equation 15], where $u^+(\mathbf{x}, \omega)$ is the acoustic wavefield (with the oscillatory component reduced) propagating in the positive x_1 direction, $\mathbf{x} = (x_1, x_2)$ is the space coordinate, $\partial_i = \partial/\partial x_i$, $k = \omega/c$, $\epsilon(\mathbf{x}) = (\omega^2/(k_0^2 c^2(\mathbf{x})) - 1)$, $k_0 = \omega/c_0$ is the reference phase and $c(\mathbf{x})$ is the spatially variable acoustic velocity. For homogeneous media k_0 is chosen so that $\epsilon(\mathbf{x})$ vanishes and for heterogeneous media k_0 is chosen so that the spatial average of $\epsilon(\mathbf{x})$ is small. Equation (1) assumes

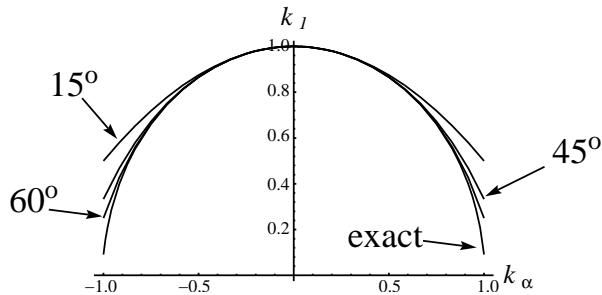


Figure 1: Dispersion curves for various one-way wave equations [modified from 49, Figure 9.3].

the medium is weakly heterogeneous and the scale-lengths of the heterogeneities are large relative to the radiation wavelengths.

These parabolic approximations can also be derived by a plane-wave argument [48]. The exact dispersion relation is obtained by substituting the plane-wave solution $\exp i[\omega t + \mathbf{k} \cdot \mathbf{x}]$ into the wave equation, where t is time and \mathbf{k} is the wavenumber vector. For homogeneous media and 2D problems, the dispersion relation for the full acoustic wave equation takes the form

$$\mathbf{k}^2 = k_1^2 + k_2^2 = \frac{\omega^2}{c^2} . \quad (2)$$

Equation (2) provides a relationship between the frequency and wavenumber of the plane-wave, and the medium properties (i.e., wave velocity c). Choosing the x_1 -axis to be the preferred direction of propagation, the corresponding wavenumber component k_1 can be approximated by an expansion in the lateral component. The parabolic approximation to the wave equation is then obtained by applying the Fourier derivative rule $k_i \iff -i\partial_i$ to the approximate dispersion relation. For example, the approximation

$$k_1 \approx \frac{\omega}{c} - \frac{ck_2^2}{2\omega} \quad (3)$$

is derived from a rearrangement of equation (2), followed by a binomial (Taylor series) expansion [see 46]. Applying the Fourier derivative rule to equation (3) and extracting a reference phase $k_0 = \omega/c_0$ gives equation (1).

For accurate results with these equations, the propagation path of the wave-field is limited to an angular aperture centred about the preferred direction of propagation. The size of the aperture is dependent on the accuracy of the dispersion approximation and so only a limited angular range of forward diffraction can be modeled. For instance, the so-called 45° approximation

$$k_1 = \frac{\omega}{c} - \frac{k_2^2}{2\frac{\omega}{c} - \frac{ck_2^2}{2\omega}} \quad (4)$$

is accurate for propagation angles up to about $\pm 45^\circ$ from the preferred direction of propagation and is derived using a continued fraction expansion [see 46, pp. 76–78]. Figure 1 displays various approximations to the dispersion relation and indicates that higher order expansions are indeed more accurate. However, these higher order expansions generally involve more complicated one-way wave equations. For elastic waves, this approach is further restricted to problems where only one identifiable propagation mode exists and mode coupling due to inhomogeneities is assumed weak and negligible. Regardless of these restrictions, the parabolic approximation is technically valid to a greater degree than zeroth-order geometrical ray theory [45]. This is because these one-way equations allow lateral variations of the medium on a sub-Fresnel zone level, whereas ray theory requires that the medium be smooth within this zone. Thus the one-way wave equation supersedes ray theory, at least in terms of modeling lateral diffractions.

Practical limitations of these one-way wave equations can sometimes be difficult to evaluate. For example, it was discovered that the standard 15° parabolic approximation [i.e., equation (15) in 24] failed to position migrated images correctly in the presence of lateral variations [50; 51; 52]. This failure was attributed to the omission of a so-called ‘thin-lens’ term when simplifying the acoustic wave equation [see 52]. This problem was later corrected by [46] by estimating the omitted term and this led to the 45° one-way ‘migration’ equation (4). One could argue, however, that the particular 15° parabolic approximation was improperly applied to the specific problem in the first place and this highlights the importance of thoroughly understanding the limitations of any given method. Fortunately, various approaches are available to improve the accuracy as well as to optimize these parabolic approximations. As discussed earlier, equation (4) is one such improvement, which involves a replacement of the Taylor series expansion of the dispersion relation by a Padé or rational approximation [e.g., 53]. [54] have shown that higher order extensions of the standard parabolic equation can be implemented effectively and produce surprisingly accurate results for the acoustic case.

A different approach to the parabolic approximation involves an operator technique proposed by [55], which was used to approximate the Helmholtz equation for wide-angle light propagation in optical fibers. This approach involves splitting (or factoring) the wave equation into two parts, followed by an approximation of the ‘operator-root’. In a notation similar to theirs, the Helmholtz equation for the transverse component $E(\omega, x_1, x_\alpha)$ of the electric field in three-dimensional (3D) media with laterally variable refractive index $n(\omega, x_\alpha)$ is written

$$\partial_1^2 E + \partial_\alpha^2 E + \frac{\omega^2}{c^2} n^2(\omega, x_\alpha) E = 0 , \quad (5)$$

where $\partial_\alpha^2 = \partial^2/\partial x_2^2 + \partial^2/\partial x_3^2$ and $x_\alpha = (x_2, x_3)$ are the lateral space coordinates. Equation (5) has the formal solution

$$E(\Delta x_1, x_\alpha) = \exp \left[\pm i \Delta x_1 \left(\partial_\alpha^2 + \frac{\omega^2}{c^2} n^2 \right)^{1/2} \right] E_0(x_\alpha) \quad (6)$$

for a single frequency, where $E_0(x_\alpha) = E(x_1 = 0, x_\alpha)$ is the initial wavefield. The derivation of this solution assumes that the medium is invariant in the x_1 direction. In contrast to the reference-phase approach discussed earlier, the ‘phase’ (i.e., square-root term) in equation (6) is expressed in terms of the operators of the wave equation and not the plane-wave dispersion relation. Assuming small variations in the refractive index of the fiber, the operator-root in the phase function of equation (6) can be approximated

$$\left(\partial_\alpha^2 + \frac{\omega^2}{c^2}n^2\right)^{1/2} \approx \frac{\partial_\alpha^2}{(\partial_\alpha^2 + k^2)^{1/2} + k} + k + k\left(\frac{n}{n_0} - 1\right), \quad (7)$$

where $k = n_0\omega/c$ and n_0 is the reference medium refractive index. This approximation is valid only for a properly chosen reference medium (i.e., n_0 and c_0). Since the only assumption involved is that of weak heterogeneity, this approximation is accurate for wide angles of propagation and, in fact, is exact for homogeneous media. It is interesting to note that this approach relates closely to the phase-screen method [e.g., 27; 28]. [56] applied the above operator technique along with two other approximations to the operator-root, but for the acoustic wave equation. These approximations were implemented within the acoustic split-step computer algorithm of [25] so that the accuracies of all three operator-root approximations could be compared. Their results indicated that the wider angle parabolic equation of [55] was least sensitive to the choice of reference phase and least effected by phase errors.

[57] further improves the above operator approach for wider angles of propagation. This is done by introducing the ‘rational linear square-root’ and involves applying the Padé approximation

$$x^{1/2} \approx \frac{a_0 + a_1x}{1 + b_1x} \quad (8)$$

to the operator-root. The coefficients a_0, a_1 and b_1 are real and chosen to fit optimally the square-root function. In [58] the authors demonstrate that the real coefficients of this rational linear approximation improperly treat the evanescent waves that can propagate within waveguides. Evanescent waves have complex wavenumbers and so their amplitudes can either grow or decay exponentially with propagation distance. Growing evanescent waves are particularly problematic for numerical algorithms, as their amplitudes may overshadow the signals of interest. To correct this problem [58] modify the ‘bilinear square-root’ approximation (8) and extend this method to elastic waves. The bilinear approximation is modified by replacing the real coefficients with complex coefficients. In [58] the authors show that their bilinear approximation not only propagates the complex modes within the waveguide more accurately, but also allows for improved numerical stability of ordinary waves. Unfortunately, all of the above approaches are limited when applied to elastic media. In contrast to acoustic media, where only one body-wave mode exists, isotropic elastic solids allow two wave modes. Thus application of these approaches requires choosing one wave mode and neglecting the other. This is unacceptable because coupling between

wave modes can be important, especially at interfaces or for long propagation distances.

[59] and [60] introduce higher order Padé series expansions to the split-operators which allow even wider angles of propagation. More importantly though, these higher order expansions allow wave speeds to differ substantially from the chosen reference speed (or phase). In other words, the restriction that wave speeds be close to the reference speed does not apply and so these approximations can model weak coupling between wave modes. Although these higher order expansions of the split-operator assume the medium is isotropic and homogeneous (in fact range independent), they can be applied to weak range dependence if the medium is approximated by a sequence of range independent regions [61]. However, the range dependent solution may be inaccurate for problems involving abrupt boundaries, where the assumption of weak heterogeneity does not apply. This approach was further extended to transversely-isotropic (TI) media by [62].

The reference phase approach discussed earlier involves a ‘localization’ of an exact non-local operator and hence propagation is explicitly restricted to narrow angles as well as weak and slowly varying inhomogeneous media. Unfortunately these restrictions are frequently violated in seismological applications. The operator technique proposed by [55] is an improvement upon the reference phase approach because it does not involve a localization of the wave equation operator. However, this operator approach makes the explicit assumption of weak heterogeneity to obtain a ‘simple’ expression for the operator-root in terms of a perturbation series.

A significant step forward was realized by [26] who applied a similar operator-splitting approach to that of [55], but sought a more detailed and widely applicable expression for the operator-root. This permits a generalization of the one-way wave equation technique and introduces a new class of propagation algorithms. In their derivation, the exact factorization of the scalar (or acoustic) Helmholtz equation is written

$$\left[\frac{i}{k_0} \partial_1 + \left(K^2(x_\alpha) + \frac{1}{k_0^2} \partial_\alpha^2 \right)^{1/2} \right] u^+(\omega, \mathbf{x}) = 0, \quad (9)$$

where the reference wavenumber is $k_0 = \omega/c_0$, c_0 is the reference velocity, $K(x_\alpha) = c_0/c(x_\alpha)$ and $c(x_\alpha)$ is the laterally varying velocity. This equation is exact for forward propagation when there is no range dependence, since range variations (i.e., material inhomogeneities) are necessary to couple the forward and reverse propagating waves [35]. However, this approach requires a formal expression for the operator-root in equation (9) and the means of evaluating this operator-root are not trivial.

More general than the aforementioned methods that factor the wave solution, the derivation can still be reduced to the conventional narrow-angle parabolic approximations for media limited to weak inhomogeneities and weak gradients. More importantly though, the restriction of weak lateral inhomogeneity can be dropped and wider angles of propagation are also allowed. The factoriza-

tion (9) involves a ‘pseudo-differential operator’ (i.e., the operator-root) and an expression for this is sought in the lateral Fourier transform domain (pseudo-differential operators and their Fourier representation will be discussed in the subsequent section). Simplification of the resulting operator-root expression involves introducing an asymptotic solution or ‘high-frequency’ approximation. In the context of geometrical optics or ray theory, the high-frequency assumption generally implies that the wavefield is localized in space. In this approach, however, the high-frequency approximation is applied to the Fourier representation or ‘symbol’ of the pseudo-differential cross-range operator. Since the asymptotic solution retains some of the global properties of the cross-range operator, some full waveform effects are included, at least for the frequency range of interest.

3 Theory behind ‘splitting’ the wave equation

The problem of reconstructing the Earth’s subsurface requires the ability to model the transmission as well as the reflection of waves. From a mathematical point of view, it amounts to an inverse scattering problem [63], and requires including the interaction or coupling between the forward and reverse waves due to inhomogeneities. [63] introduced a 6×6 matrix parabolic formulation for orthorhombic elastic media that includes the effects of reverse scattering. This 6×6 matrix representation is referred to as a ‘displacement-stress’ formulation and is convenient when dealing with boundary-value (i.e., reflection/transmission) problems [e.g., 15; 64]. The formulation of [63] uses an operator-splitting approach similar to that of [26] and was subsequently reduced to the acoustic wave equation [65; 66]. In this approach, the forward and reverse wave coupling is approximated using an iterative process based on a generalization of the Born method (which they refer to as a Bremmer or Neumann series summation). In seismology, this iterative approach to coupling was already known to be an efficient method of numerically solving the scattering problem [e.g., 67]. Application of this parabolic approximation to various multiple scattering examples is presented in [68], where its potential role in migration algorithms is discussed.

For many applications, however, it is not imperative to consider the complete transmission and reflection of waves, and it may be only necessary to model the transmission response [i.e., for full-wave inversion 69]. [36] introduces a hierarchy of one-way wave equations based on a 3×3 matrix factorization of the elastic wave equation for 3D, generally-anisotropic, heterogeneous media. The matrix formulation allows parallels to be drawn with conventional ray-based approaches, and can be reduced to a path-integral representation or to the standard ray limit via the stationary phase approximation [see 36]. This approach simulates one-way propagation of elastic (and potentially visco-elastic) waves in generally anisotropic media which are smoothly variable and neglects backscatter. Although these wave equations are based on a 3×3 displacement formulation, it is still possible to include the coupling between forward and reverse propagating waves [see 41, for the acoustic case]. For the transmission

problem [40] shows that accurate amplitudes can be calculated in the presence of strong gradients based on energy–flux considerations. The major strength of this formulation is that this elastic one–way seismic wavefield extrapolator is more generally applicable than ray methods, primarily because it can handle robustly transitions from weak–to–strong or arbitrary anisotropy. For example, within the vicinity of a conical–point singularity the polarization vectors of the qS–waves vary rapidly and are singular at the acoustic axis. However, the propagator remains smooth around and at the acoustic axis. Thus, singularities associated with anisotropic material can be accounted for without special attention.

The indicial form of the anisotropic elastic wave equation for a single frequency ω is written

$$\partial_j(c_{ijkl}\partial_k u_l) + \omega^2 \rho u_i = 0, \quad (10)$$

where u_i is the i –th component of displacement ($i = 1, 2, 3$), ρ is density and c_{ijkl} is the 81–component tensor of elastic constants, which reduces to 21 independent components by the symmetries $c_{ijkl} = c_{jikl} = c_{ijlk} = c_{klij}$ [70]. It is understood that Cartesian coordinates x_i are being used. The preferred direction of propagation is taken to be along the x_1 –axis and the lateral– (or cross–, tangential–, transverse–) coordinates are x_α , where $\alpha = 2, 3$. Throughout, Greek subscripts will be reserved for the lateral coordinates.

If we considering a single transverse slowness (i.e., single plane–wave) for two reasons: (i) since the coefficients of the wave equation are constant for homogeneous media, the exact solution to the one–way operator for more general wavefields can be found by the method of plane–wave integration over lateral slowness and (ii) an understanding of the one–way operator for a single plane–wave will enable a clear presentation of some of the key concepts. This will not only be helpful when discussing the more complicated factorization of the wave equation for inhomogeneous media, but will allow parallels to be drawn between the approximate operator for inhomogeneous media and the exact operator for homogeneous media. In fact, a geometrical appreciation of the physical action of the plane–wave operator results by considering homogeneous media.

3.1 Elastic homogeneous case

For homogeneous media equation (10) may be rewritten

$$[\mathbf{C}_{11}\partial_1^2 + (\mathbf{C}_{\alpha 1} + \mathbf{C}_{1\alpha})\partial_\alpha\partial_1 + \mathbf{C}_{\alpha\beta}\partial_\alpha\partial_\beta + \omega^2\rho] \mathbf{u} = 0, \quad (11)$$

where $(\mathbf{C}_{jk})_{il} = c_{ijkl}$. Grouping terms and considering only the single plane–wave $\mathbf{u}(\mathbf{x}) = \tilde{\mathbf{u}}(x_1) \exp[i\omega p_\alpha x_\alpha]$ with lateral slowness p_α , equation (11) becomes

$$[(\partial_1 + i\omega\mathbf{A})^2 + \omega^2\mathbf{B}] \tilde{\mathbf{u}}(x_1) = 0, \quad (12)$$

where

$$\mathbf{A} = \frac{1}{2}\mathbf{C}_{11}^{-1}(\mathbf{C}_{\alpha 1} + \mathbf{C}_{1\alpha})p_\alpha \quad (13)$$

and

$$\mathbf{B} = \mathbf{A}^2 - \mathbf{C}_{11}^{-1} \mathbf{C}_{\alpha\beta} p_\alpha p_\beta + \rho \mathbf{C}_{11}^{-1} . \quad (14)$$

Equation (12) is a second order partial differential equation in x_1 and describes exactly both the forward and reverse propagating waves in homogeneous, anisotropic media.

To help in the interpretation of the matrices \mathbf{A} and \mathbf{B} as well as aid in the derivation of an appropriate factorization of the wave equation, it is instructive to present the ray-theory Christoffel equation. Substituting the plane-wave $u_l(x_i) = g_l \exp[i\omega p_i x_i]$ into equation (10) and assuming homogeneity yields

$$(c_{ijkl} p_j p_k - \rho \delta_{il}) g_l = 0 , \quad (15)$$

where δ_{il} is the Dirac δ -function, p_i is the slowness vector normal to the wavefront $\tau(x_i)$ and g_l is the polarization vector. Equation (15) is referred to as the ray-theory Christoffel equation [8]. A nontrivial solution for the polarization g_l requires that

$$\det |a_{ijkl} n_j n_k - v_n^2 \delta_{il}| = 0 , \quad (16)$$

where a_{ijkl} is the density-normalized elastic tensor, $n_i = p_i v_n$ is the wave normal and v_n is the phase (or normal) velocity. Now, taking the same approach but substituting the plane-wave $\mathbf{u}(x_1) = \mathbf{g} \exp[i\omega p_1 x_1]$ into equation (12) yields

$$\mathbf{B} \mathbf{g} = (p_1 \mathbf{I} + \mathbf{A})^2 \mathbf{g} . \quad (17)$$

It can be seen that equation (17), when compared to equation (15), is analogous to the ray-theory Christoffel equation. For each choice of the pair $p_\alpha = (p_2, p_3)$ there is an allowed maximum of six values of $p_1 = P_1^{(m)}(p_\alpha)$ and six corresponding eigen-polarizations $\mathbf{g}^{(m)}$, where $m = 1 - 6$. For a given vertical slowness there are six possible horizontal slownesses: three positive slownesses corresponding to the forward propagating qP-, qS₁ and qS₂-waves (i.e., propagating in the positive direction of the horizontal axis); and three negative slownesses corresponding to the reverse propagating body-waves. For each horizontal slowness, there is a corresponding polarization or eigen-polarization \mathbf{g} . Thus, for a given allowable slowness (p_1, p_α) , the ‘one-way Christoffel’ equation (17) describes the propagation characteristics (i.e., polarization and phase velocity) of the corresponding plane-wave mode.

From equation (17), the following expression may be inferred

$$\mathbf{B}^{\frac{1}{2}} = \pm (p_1 \mathbf{I} + \mathbf{A}) , \quad (18)$$

which relates the slowness p_1 to the matrices \mathbf{A} and \mathbf{B} . The positive and negative square roots in equation (18) might be expected to correspond to the forward and reverse propagating plane-waves with slowness p_1 , respectively. Here and in the remaining discussion, forward propagation refers to propagation

in the positive x_1 -direction. It is important to note that equation (18) is not an exact, but rather a suggested expression for the square-root of matrix \mathbf{B} .

Moving all terms of the positive root in equation (18) to one side and applying the Fourier derivative rule $p_1 \iff \partial_1/i\omega$ implies

$$\left(\partial_1 \mathbf{I} + i\omega \mathbf{A} - i\omega \mathbf{B}^{\frac{1}{2}}\right) = 0 . \quad (19)$$

Expression (19) is an operator which, when acting upon $\tilde{\mathbf{u}}(x_1)$, describes the forward propagation (i.e., propagation in the positive x_1 -direction) of a plane-wave. Thus, the solution to the differential equation (12) can be given by a linear combination of terms like $\tilde{\mathbf{u}}(x_1) = \mathbf{g}^{(n)} \exp[i\omega P_1^{(n)} x_1]$ for forward travelling waves, where $n = 1, 3$.

Without assuming equation (18), but taking guidance from equation (19), the full wave equation (12) is factored according to

$$\left[\left(\partial_1 + i\omega \mathbf{A} + i\omega \mathbf{B}^{\frac{1}{2}}\right) \left(\partial_1 + i\omega \mathbf{A} - i\omega \mathbf{B}^{\frac{1}{2}}\right) - \omega^2 [\mathbf{A}, \mathbf{B}^{\frac{1}{2}}]\right] \tilde{\mathbf{u}}(x_1) = 0 , \quad (20)$$

which consists of two operators that are first-order in x_1 and a commutator term $[\mathbf{A}, \mathbf{B}^{1/2}] = \mathbf{A}\mathbf{B}^{1/2} - \mathbf{B}^{1/2}\mathbf{A}$. For a properly chosen $\mathbf{B}^{1/2}$, the factor

$$\left(\partial_1 + i\omega \mathbf{A} - i\omega \mathbf{B}^{\frac{1}{2}}\right) \tilde{\mathbf{u}}(x_1) = 0 \quad (21)$$

is the exact one-way wave equation for forward travelling waves in homogeneous media. However, the correct form of the matrix square-root $\mathbf{B}^{1/2}$ in equation (21) is still unknown and, hence, an expression of this operator-root is now sought.

A correct expression for the square-root of matrix \mathbf{B} can be found by first introducing the 3×3 eigenvector matrix \mathbf{G} and diagonal eigenvalue matrix \mathbf{P}_1 . The columns of \mathbf{G} are given by the three allowed polarizations (or eigendisplacements) of the forward propagating waves and the diagonal elements of \mathbf{P}_1 are the corresponding x_1 -components of slowness. Since equation (17) is an expression for an individual plane-wave mode, a more complete expression is necessary, one that includes the description of all three body-waves. This is accomplished by considering a system of equations based on equation (17) for each individual forward propagating body-wave. Thus, introducing \mathbf{G} and \mathbf{P}_1 for \mathbf{g} and p_1 in equation (17) yields

$$\mathbf{B}\mathbf{G} = \mathbf{G}\mathbf{P}_1^2 + \mathbf{A}^2\mathbf{G} + 2\mathbf{A}\mathbf{G}\mathbf{P}_1 , \quad (22)$$

which is an augmented form of the Christoffel equation (17) and describes the forward propagation of all three body-waves. The polarization vectors or eigenvectors for all three body-waves are evaluated using the common lateral slowness p_α and so they are not exactly orthogonal. However, these eigenvectors are not collinear and so the matrix \mathbf{G} is invertible.

Isolating the matrix \mathbf{B} , equation (22) may be rewritten

$$\mathbf{B} = (\mathbf{G}\mathbf{P}_1\mathbf{G}^{-1} + \mathbf{A})^2 + [\mathbf{A}, \mathbf{G}\mathbf{P}_1\mathbf{G}^{-1}] . \quad (23)$$

Assuming for now that the commutator term on the right is negligible,

$$[\mathbf{A}, \mathbf{G}\mathbf{P}_1\mathbf{G}^{-1}] \approx 0, \quad (24)$$

an approximation to the square-root of the matrix \mathbf{B} is seen to be given by

$$\mathbf{B}^{\frac{1}{2}} \approx \mathbf{G}\mathbf{P}_1\mathbf{G}^{-1} + \mathbf{A}. \quad (25)$$

Substituting this approximate root into the forward factor (21) yields

$$(\partial_1 - i\omega\mathbf{G}\mathbf{P}_1\mathbf{G}^{-1}) \tilde{\mathbf{u}}(x_1) = 0, \quad (26)$$

which represents the one-way wave equation for a forward travelling plane-wave in homogeneous, anisotropic media.

The key step in factoring the full wave equation involves neglecting the commutator terms in equations (20) and (23). The primary motivation for neglecting these commutator terms was based on an assumption used in conventional one-way approximations discussed earlier. Specifically, this assumption is the narrow-angle approximation and translates to assuming that p_α is small. In equation (20), the commutator term is of order $O(p_\alpha)$, whereas the two operators are of order $O(1)$. In equation (23), the commutator term is also of order $O(p_\alpha)$, whereas the squared term is of order $O(p_\alpha^2)$. Thus, for small p_α , the commutator terms in both equations can be neglected. Thus, it would appear that the operator-root approximation (25) and the one-way wave equation (26) are only accurate when the range of propagation is limited to small p_α . However, it turns out below that equation (26) is, in fact, the exact one-way wave equation for forward propagating plane-waves for all allowable p_α .

The reason that the one-way wave equation (26) is an exact factor of equation (12) can be seen by substituting the exact form of the matrix \mathbf{B} (23) into equation (12), giving

$$\begin{aligned} & \left[(\partial_1 + i\omega\mathbf{A})^2 + \omega^2 (\mathbf{G}\mathbf{P}_1\mathbf{G}^{-1} + \mathbf{A})^2 + \omega^2 [\mathbf{A}, \mathbf{G}\mathbf{P}_1\mathbf{G}^{-1}] \right] \tilde{\mathbf{u}}(x_1) = 0 \\ & = (\partial_1 + 2i\omega\mathbf{A} + i\omega\mathbf{G}\mathbf{P}_1\mathbf{G}^{-1}) (\partial_1 - i\omega\mathbf{G}\mathbf{P}_1\mathbf{G}^{-1}) \tilde{\mathbf{u}}(x_1) \quad .(27) \end{aligned}$$

The final expression in equation (27) is obtained by factoring the first two squared terms and noting that the commutator terms cancel. It is interesting to note that the right and left factors in equation (27) are ‘asymmetric’, where the term $2i\omega\mathbf{A}$ appears in the left but not the right factor. Equation (26) is the exact one-way wave equation for forward propagating plane-waves and so, for homogeneous media and properly chosen initial conditions, the right factor in equation (27) operating on the wavefield $\tilde{\mathbf{u}}(x_1)$ will always equal zero. However, when the initial conditions are not properly chosen (e.g., when the wavefield $\tilde{\mathbf{u}}(x_1)$ contains some reverse propagating components), the right factor operating on $\tilde{\mathbf{u}}(x_1)$ does not equal zero. However, the left factor serves as a ‘corrector’ term by annihilating this error. Therefore, an exact plane-wave solution to equation (26) for forward propagating waves is given by $\tilde{\mathbf{u}}(x_1) = \mathbf{G} \exp[i\omega\mathbf{P}_1x_1]\mathbf{c}$, where the three-vector \mathbf{c} represents the initial amplitudes of all three forward propagating body-waves at $x_1 = 0$.

3.2 Elastic heterogeneous case

Here discussion parallels that of the previous section, but a spectrum of transverse slownesses will be considered. For inhomogeneous media equation (10) becomes

$$[\mathbf{C}_{11}\partial_1^2 + (\mathbf{C}_{\alpha 1} + \mathbf{C}_{1\alpha})\partial_\alpha\partial_1 + \partial_i(\mathbf{C}_{i1}\partial_1 + \mathbf{C}_{i\alpha}\partial_\alpha) + \mathbf{C}_{\alpha\beta}\partial_\alpha\partial_\beta + \omega^2\rho] \mathbf{u} = 0 . \quad (28)$$

Grouping approximate terms, equation (28) may be re-written

$$\left[(\partial_1 + \mathbf{M}(\mathbf{x}, \partial_\alpha))^2 + \mathbf{N}(\mathbf{x}, \partial_\alpha; \omega) \right] \mathbf{u} = 0 , \quad (29)$$

where

$$\mathbf{M}(\mathbf{x}, \partial_\alpha) = \frac{1}{2}\mathbf{C}_{11}^{-1}(\mathbf{C}_{\alpha 1} + \mathbf{C}_{1\alpha})\partial_\alpha + \frac{1}{2}\mathbf{C}_{11}^{-1}\partial_i\mathbf{C}_{i1} , \quad (30)$$

$$\mathbf{N}(\mathbf{x}, \partial_\alpha; \omega) = \mathbf{P}_{\alpha\beta}\partial_\alpha\partial_\beta + \mathbf{Q}_\alpha\partial_\alpha + \mathbf{R} + \omega^2\mathbf{S} \quad (31)$$

and

$$\begin{aligned} \mathbf{P}_{\alpha\beta} &= \mathbf{C}_{11}^{-1} \left(\mathbf{C}_{\alpha\beta} - \frac{1}{4}(\mathbf{C}_{\alpha 1} + \mathbf{C}_{1\alpha})\mathbf{C}_{11}^{-1}(\mathbf{C}_{\beta 1} + \mathbf{C}_{1\beta}) \right) , \\ \mathbf{Q}_\alpha &= \mathbf{C}_{11}^{-1}\partial_i\mathbf{C}_{i\alpha} - \frac{1}{2}\partial_1(\mathbf{C}_{11}^{-1}(\mathbf{C}_{\alpha 1} + \mathbf{C}_{1\alpha})) , \\ \mathbf{R} &= -\frac{1}{4}(\mathbf{C}_{11}^{-1}\partial_i\mathbf{C}_{i1})^2 - \frac{1}{2}\partial_1(\mathbf{C}_{11}^{-1}\partial_i\mathbf{C}_{i1}) , \\ \mathbf{S} &= \rho\mathbf{C}_{11}^{-1} . \end{aligned} \quad (32)$$

Equation (29) is a second order partial differential equation in x_1 and describes both the forward and reverse propagating waves in inhomogeneous, anisotropic media.

Suppose that equation (31) can be written in the form

$$\mathbf{N} = \mathbf{\Lambda}^2 + \mathbf{\Delta} , \quad (33)$$

where the operators $\mathbf{\Lambda}$ and $\mathbf{\Delta}$ are to be explained later, and substituting (33) into equation (29) yields

$$\left[(\partial_1 + \mathbf{M})^2 + \mathbf{\Lambda}^2 + \mathbf{\Delta} \right] \mathbf{u} = 0 . \quad (34)$$

Taking guidance from the previous section, equation (34) will be factored according to

$$\begin{aligned} & [(\partial_1 + \mathbf{M} + i\mathbf{\Lambda})(\partial_1 + \mathbf{M} - i\mathbf{\Lambda}) - i[\mathbf{\Lambda}, (\partial_1 + \mathbf{M})] + \mathbf{\Delta}] \mathbf{u} = \\ & [(\partial_1 + \mathbf{M} + i\mathbf{\Lambda})(\partial_1 + \mathbf{M} - i\mathbf{\Lambda}) - i[\mathbf{\Lambda}, \mathbf{M}] + i[\partial_1, \mathbf{\Lambda}] + \mathbf{\Delta}] \mathbf{u} = \\ & [(\partial_1 + \mathbf{M} + i\mathbf{\Lambda})(\partial_1 + \mathbf{M} - i\mathbf{\Lambda}) - i[\mathbf{\Lambda}, \mathbf{M}] + i(\partial_1\mathbf{\Lambda}) + \mathbf{\Delta}] \mathbf{u} = 0 , \end{aligned} \quad (35)$$

where

$$[\partial_1, \mathbf{\Lambda}] \mathbf{u} = \partial_1 (\mathbf{\Lambda} \mathbf{u}) - \mathbf{\Lambda} \partial_1 \mathbf{u} = (\partial_1 \mathbf{\Lambda}) \mathbf{u} + \mathbf{\Lambda} (\partial_1 \mathbf{u}) - \mathbf{\Lambda} (\partial_1 \mathbf{u}) = (\partial_1 \mathbf{\Lambda}) \mathbf{u} . \quad (36)$$

The term $(\partial_1 \mathbf{\Lambda})$ can be ignored in equation (35) because it depends on material gradients in the x_1 direction, is lower order in ω and vanishes in the homogeneous limit. Furthermore, if $\mathbf{\Delta} = i[\mathbf{\Lambda}, \mathbf{M}]$, equation (33) can be rewritten

$$\mathbf{N} = \mathbf{\Lambda}^2 + i[\mathbf{\Lambda}, \mathbf{M}] \quad (37)$$

and the terms $-i[\mathbf{\Lambda}, \mathbf{M}]$ and $\mathbf{\Delta}$ in equation (35) cancel one another. Thus, equation (35) can be rewritten

$$[(\partial_1 + \mathbf{M} + i\mathbf{\Lambda})(\partial_1 + \mathbf{M} - i\mathbf{\Lambda})] \mathbf{u} = 0 \quad (38)$$

and consists of two operators that are first-order in x_1 . For properly chosen $\mathbf{\Lambda}$, the factor

$$(\partial_1 + \mathbf{M} - i\mathbf{\Lambda}) \mathbf{u} = 0 \quad (39)$$

represents the approximate one-way wave equation for the forward propagating waves within an inhomogeneous, anisotropic medium. The matrix $\mathbf{\Lambda}$ is analogous to the square-root matrix $\mathbf{B}^{1/2}$ for homogeneous media and is the operator-root now sought.

An expression for the operator-root $\mathbf{\Lambda}$ can be found by first rewriting equation (37) in the following form

$$\mathbf{N} + \mathbf{M}^2 = (\mathbf{\Lambda} - i\mathbf{M})(\mathbf{\Lambda} + i\mathbf{M}) , \quad (40)$$

where the right-hand side is a product of two operators relating the operator root $\mathbf{\Lambda}$ to the known matrices \mathbf{M} and \mathbf{N} . Each factor on the right represents a sum in which \mathbf{M} is a known partial differential operator and $\mathbf{\Lambda}$ is an unknown pseudo-differential operator.

The approach taken here will involve a Fourier transform domain representation of the PSDO $\mathbf{\Lambda}$. The reason for this approach is because the calculus of PSDOs can be ‘simplified’ when performed in this domain [71]. The standard-ordering PSDO form will be used in evaluating the symbols or Fourier representations of the PSDOs in equation (40). The symbols for the known matrix partial differential operators on the left-hand side of equation (40) will be evaluated first since these expression can be found exactly using basic Fourier transformation properties (e.g., the Fourier derivative rule). Next, the Fourier representation for the right-hand side of equation (40) is determined, but the process is more complicated because it involves an unknown PSDO as well as determining the symbol for the composition of two PSDOs [see 36, appendix A].

The symbols for the PDOs $\mathbf{N}(x_\alpha, \partial_\alpha; \omega)$ and $\mathbf{M}(x_\alpha, \partial_\alpha; \omega)$ are written

$$\begin{aligned} \text{sym} [\mathbf{N}(x_\alpha, \partial_\alpha; \omega)] &= \mathbf{N}(x_\alpha, p_\alpha; \omega) \\ &= -\omega^2 \mathbf{P}_{\alpha\beta} p_\alpha p_\beta + i\omega \mathbf{Q}_\alpha p_\alpha + \mathbf{R} + \omega^2 \mathbf{S} \\ &= \omega^2 \mathbf{B} + i\omega \mathbf{Q}_\alpha p_\alpha + \mathbf{R} , \end{aligned} \quad (41)$$

and

$$\begin{aligned}
\text{sym} [\mathbf{M}(x_\alpha, \partial_\alpha; \omega)] &= \mathbf{M}(x_\alpha, p_\alpha; \omega) \\
&= i\omega \mathbf{M}_\alpha(x_\alpha) p_\alpha + \mathbf{M}_0(x_\alpha) \\
&= i\omega \mathbf{A} + \mathbf{M}_0,
\end{aligned} \tag{42}$$

respectively, where

$$\mathbf{M}_0 = \frac{1}{2} \mathbf{C}_{11}^{-1} \partial_i \mathbf{C}_{i1} \quad \text{and} \quad \mathbf{M}_\alpha = \frac{1}{2} \mathbf{C}_{11}^{-1} (\mathbf{C}_{\alpha 1} + \mathbf{C}_{1\alpha}) \partial_\alpha. \tag{43}$$

Since the coefficients of the PSDO \mathbf{M} depend on position, the symbol $\text{sym} \mathbf{M}^2 \neq (\text{sym} \mathbf{M})^2$ and so it is necessary to expand the square of the PSDO $\mathbf{M}(x_\alpha, \partial_\alpha; \omega)$ as follows

$$\begin{aligned}
\mathbf{M}^2 &= (\mathbf{M}_\alpha \partial_\alpha + \mathbf{M}_0) (\mathbf{M}_\beta \partial_\beta + \mathbf{M}_0) \\
&= \mathbf{M}_\alpha \mathbf{M}_\beta \partial_\alpha \partial_\beta + \mathbf{M}_\alpha (\partial_\alpha \mathbf{M}_\beta) \partial_\beta + \mathbf{M}_\alpha \mathbf{M}_0 \partial_\alpha + \mathbf{M}_\alpha (\partial_\alpha \mathbf{M}_0) \\
&\quad + \mathbf{M}_0 \mathbf{M}_\beta \partial_\beta + \mathbf{M}_0^2.
\end{aligned} \tag{44}$$

The symbol of equation (44) can be written

$$\begin{aligned}
\text{sym} [\mathbf{M}^2] &= \mathbf{M}_\alpha \mathbf{M}_\beta (i\omega)^2 p_\alpha p_\beta + \mathbf{M}_\alpha (\partial_\alpha \mathbf{M}_\beta) i\omega p_\beta + \mathbf{M}_\alpha \mathbf{M}_0 i\omega p_\alpha \\
&\quad + \mathbf{M}_\alpha (\partial_\alpha \mathbf{M}_0) + \mathbf{M}_0 \mathbf{M}_\beta i\omega p_\beta + \mathbf{M}_0^2.
\end{aligned} \tag{45}$$

Squaring the symbol (42)

$$\begin{aligned}
(\text{sym}[\mathbf{M}])^2 &= (i\omega \mathbf{M}_\alpha p_\alpha + \mathbf{M}_0) (i\omega \mathbf{M}_\alpha p_\beta + \mathbf{M}_0) \\
&= \mathbf{M}_\alpha \mathbf{M}_\beta (i\omega)^2 p_\alpha p_\beta + \mathbf{M}_0 \mathbf{M}_\beta i\omega p_\beta + \mathbf{M}_\alpha \mathbf{M}_0 i\omega p_\alpha \\
&\quad + \mathbf{M}_0^2,
\end{aligned} \tag{46}$$

equation (45) can be rewritten

$$\begin{aligned}
\text{sym} [\mathbf{M}^2] &= (\text{sym}[\mathbf{M}])^2 + i\omega \mathbf{M}_\alpha \partial_\alpha \mathbf{M}_\beta p_\beta + \mathbf{M}_\alpha \partial_\alpha \mathbf{M}_0 \\
&= \mathbf{M}^2(x_\alpha, p_\alpha) + i\omega \mathbf{M}_\alpha \partial_\alpha \mathbf{M}_\beta p_\beta + \mathbf{M}_\alpha \partial_\alpha \mathbf{M}_0.
\end{aligned} \tag{47}$$

Thus, the symbol of the left-hand side of equation (40) in the Fourier transform domain may be written

$$\mathbf{N}(x_\alpha, p_\alpha) + \mathbf{M}^2(x_\alpha, p_\alpha) + i\omega \mathbf{M}_\alpha \partial_\alpha \mathbf{M}_\beta p_\beta + \mathbf{M}_\alpha \partial_\alpha \mathbf{M}_0. \tag{48}$$

Turning to the right-hand side of equation (40), the symbol for the operator \mathbf{M} has already been determined, whereas the symbol for the operator-root $\mathbf{\Lambda}$ has yet to be determined. A difficulty arises here, as it is the space domain expression of the operator-root which is unknown and sought. To determine its symbol $\mathbf{\Lambda}(x_\alpha, p_\alpha)$, the right-hand side of equation (40) is rewritten using the

‘standard operator compound symbol formula’ [equation (A20b) in 36]. Specifically, it is written

$$\begin{aligned} \text{sym}[(\mathbf{\Lambda}(x_\alpha, \partial_\alpha) - i\mathbf{M}(x_\alpha, \partial_\alpha))(\mathbf{\Lambda}(x_\alpha, \partial_\alpha) + i\mathbf{M}(x_\alpha, \partial_\alpha))] = \\ \exp[i\omega^{-1}D_{y_\alpha}D_{p_\alpha}](\mathbf{\Lambda}(x_\alpha, p_\alpha) - i\mathbf{M}(x_\alpha, p_\alpha)) \\ (\mathbf{\Lambda}(y_\alpha, q_\alpha) + i\mathbf{M}(y_\alpha, q_\alpha))|_{(y_\alpha, q_\alpha) \rightarrow (x_\alpha, p_\alpha)}, \end{aligned} \quad (49)$$

where $D_{x_\alpha} = -i\partial/\partial x_\alpha$, $D_{p_\alpha} = -i\partial/\partial p_\alpha$ and summation over α is implied.

An exact expression for the symbol of the operator-root $\mathbf{\Lambda}$ is not practical (or even tractable) and so an approximation is sought in terms of some perturbation or iterative expansion to the right-hand side of equation (49). It is important while expanding this right-hand term to consider not only the material gradients, but also the frequency dependence. Since transient or impulsive solutions to the wave equation are of interest, an approximation to the root is sought in the form of an asymptotic expansion

$$\mathbf{\Lambda}(x_\alpha, p_\alpha; \omega) = \sum_{j=0}^{\infty} \omega^{-j+1} \mathbf{\Lambda}_j(x_\alpha, p_\alpha; \omega). \quad (50)$$

Substitution of the asymptotic series (50) for $\mathbf{\Lambda}$ and applying a Taylor series expansion to the exponential term in equation (49) yields

$$\begin{aligned} \left(1 + \frac{i}{\omega}D_{y_\alpha}D_{p_\alpha} + O\left(\frac{1}{\omega^2}\right)\right) (\omega\mathbf{\Lambda}_0 + \mathbf{\Lambda}_1 + \omega\mathbf{M}_\alpha p_\alpha - i\mathbf{M}_0 + O\left(\frac{1}{\omega}\right))_{x_\alpha, p_\alpha} \\ (\omega\mathbf{\Lambda}_0 + \mathbf{\Lambda}_1 - \omega\mathbf{M}_\alpha q_\alpha + i\mathbf{M}_0 + O\left(\frac{1}{\omega}\right))_{y_\alpha, q_\alpha}. \end{aligned} \quad (51)$$

Matching the leading ω^2 terms in equation (51) and (48) gives the following expression

$$\mathbf{B} = \mathbf{\Lambda}_0^2 + [\mathbf{A}, \mathbf{\Lambda}_0] \quad (52)$$

for $\mathbf{\Lambda}_0$. On comparing equations (52) and (23) an approximation of the operator-root, to leading order in ω^2 , is seen to be given by

$$\mathbf{\Lambda}_0(x_\alpha, p_\alpha) = \mathbf{G}\mathbf{P}_1\mathbf{G}^{-1} + \mathbf{A}. \quad (53)$$

Returning to the one-way wave equation (39), the Fourier transform domain representation is explicitly written

$$\begin{aligned} F[(\partial_1 + \mathbf{M} - i\mathbf{\Lambda})\mathbf{u}(y_\alpha)] \approx \\ i\omega \int (p_1 - \mathbf{G}\mathbf{P}_1\mathbf{G}^{-1})\mathbf{u}(y_\alpha) \exp[-i\omega p_\alpha y_\alpha] dy_\alpha = 0, \end{aligned} \quad (54)$$

where $\text{sym}[\partial_1] = i\omega p_1$. This approximate one-way wave equation is obtained by neglecting the lower order ω terms. That is, $\text{sym}[\mathbf{M}] \simeq i\omega\mathbf{A}$ and $\text{sym}[\mathbf{\Lambda}] \simeq \omega\mathbf{\Lambda}_0 = \omega(\mathbf{G}\mathbf{P}_1\mathbf{G}^{-1} + \mathbf{A})$.

Rearranging equation (54)

$$\int i\omega p_1 \mathbf{u}(y_\alpha) \exp[-i\omega p_\alpha y_\alpha] dy_\alpha = \int i\omega \mathbf{G} \mathbf{P}_1 \mathbf{G}^{-1} \mathbf{u}(y_\alpha) \exp[-i\omega p_\alpha y_\alpha] dy_\alpha \quad (55)$$

and applying the inverse Fourier transform from p - to x -space, equation (55) yields the explicit integral formulation of the frequency domain one-way wave equation

$$\partial_1 \mathbf{u} = i\omega \left(\frac{\omega}{2\pi}\right)^2 \int \int \mathbb{P}(x_\alpha, p_\alpha) \exp[i\omega(x_\alpha - y_\alpha)p_\alpha] \mathbf{u}(y_\alpha) dy_\alpha dp_\alpha, \quad (56)$$

where the (x_α, p_α) -dependent propagator is defined by

$$\mathbb{P}(x_\alpha, p_\alpha) = \mathbf{G} \mathbf{P}_1 \mathbf{G}^{-1}. \quad (57)$$

Equation (56) is conceptually attractive because its action is easily understood in a geometric sense. The wavefield is first decomposed into local plane-waves by the Fourier transform of the variable \mathbf{y} . The matrix \mathbf{G}^{-1} resolves the complete field into the individual plane-wave modes (i.e., qP- and qS-waves). The diagonal slowness matrix \mathbf{P}_1 defines the rate of advance of these plane-waves in the x_1 direction. The matrix \mathbf{G} then reconstitutes the individual modes back into the total field. Finally, summation over slowness (p_α) reconstructs the curved wavefronts.

This equation can correctly describe the zeroth-order ray theory, Maslov and Kirchhoff-like representations including rays which range widely over x_α and p_α . More importantly, it describes the coupling between wave modes in media exhibiting not only strong anisotropy but also weak anisotropy. Furthermore, it is capable of modeling coupling for wave propagation directions near slowness surface singularities. This is mainly due to the form of the propagator which is slowly varying even when there are rapid variations of the individual eigenvector columns of \mathbf{G} . However, the solution to this equation requires very fine sampling of the integrals for accurate numerical evaluation and hence is not computationally practical for routine use on small desktop computers.

3.3 Practical implementation

3.3.1 Narrow-angle approximation

Equation (56) is valid for wide angles as the derivation makes no explicit assumptions about p_α being small. For many practical scenarios only a limited range of p_α is needed and so further approximations to equation (56) are possible. For narrow angles, an approximation to the propagator matrix \mathbb{P} can be obtained from a Taylor series expansion about p_α of the form

$$\mathbb{P} \approx \mathbf{P}_0 + \mathbf{P}_\alpha p_\alpha + \mathbf{P}_{\alpha\beta} p_\alpha p_\beta. \quad (58)$$

This narrow-angle approximation should be appropriate when the incident wave is near planar or gently curved. The ‘subpropagator’ matrices \mathbf{P}_0 , \mathbf{P}_α and $\mathbf{P}_{\alpha\beta}$

are determined by substitution into the defining equation (52) and matching powers of p_α . The first few terms necessary for the narrow-angle (15°) approximation are given by

$$\mathbf{P}_0 = \sqrt{\rho \mathbf{C}_{11}^{-1}}, \quad (59)$$

$$\mathbf{P}_0 \mathbf{P}_\alpha + \mathbf{P}_\alpha \mathbf{P}_0 = -\mathbf{C}_{11}^{-1} (\mathbf{C}_{1\alpha} + \mathbf{C}_{\alpha 1}) \mathbf{P}_0, \quad (60)$$

$$\mathbf{P}_0 \mathbf{P}_{\alpha\beta} + \mathbf{P}_{\alpha\beta} \mathbf{P}_0 = -\mathbf{C}_{11}^{-1} \mathbf{C}_{\alpha\beta} - \mathbf{C}_{11}^{-1} (\mathbf{C}_{1\alpha} + \mathbf{C}_{\alpha 1}) \mathbf{P}_\beta - \mathbf{P}_\alpha \mathbf{P}_\beta. \quad (61)$$

The matrix \mathbf{C}_{11} is real and symmetric, and for isotropic media reduces to a diagonal matrix whose elements relate closely to the inverse wavespeeds [64]. The eigensolution of \mathbf{C}_{11} must be known to construct the symmetric matrix \mathbf{P}_0 . The ‘higher-order’ propagators (60) and (61) require the solution to nine simultaneous equations of the nine elements as well as the inversion of a 9×9 matrix constructed from \mathbf{P}_0 . However, an alternative approach is used that is based on the symmetry properties of \mathbf{P}_0 . For instance, the difference between equation (60) and its transpose leads to three independent equations for the antisymmetric part of \mathbf{P}_α . Adding equation (60) and its transpose leads to six equations for the symmetric part of \mathbf{P}_α .

Substitution of the narrow-angle propagator (58) into the integral equation (56) and noting that $\partial_\alpha \Leftrightarrow i\omega p_\alpha$ yields the frequency domain narrow-angle one-way wave equation

$$\partial_1 \mathbf{u} = i\omega \mathbf{P}_0 \mathbf{u} + \mathbf{P}_\alpha \partial_\alpha \mathbf{u} + \frac{1}{i\omega} \mathbf{P}_{\alpha\beta} \partial_\alpha \partial_\beta \mathbf{u}. \quad (62)$$

The time domain equivalent is further obtained by noting that $\partial_t \Leftrightarrow i\omega$ and is written

$$\partial_1 \partial_t \mathbf{u} = -\mathbf{P}_0 \partial_t^2 \mathbf{u} + \mathbf{P}_\alpha \partial_\alpha \partial_t \mathbf{u} - \mathbf{P}_{\alpha\beta} \partial_\alpha \partial_\beta \mathbf{u}. \quad (63)$$

These narrow-angle approximations to the one-way wave equation lend themselves to solution by FD methods and are computationally more efficient than the integral equation (56).

[41] derives a true amplitude 3D wide-angle one-way acoustic wave equation by including both the first and second order inverse frequency (ω^{-1}) terms in the asymptotic expansion of the acoustic operator root, where the importance of including the higher order energy-flux term (i.e., the second term in the asymptotic expansion of the operator root) is discussed. It is shown that the inclusion of the energy-flux term not only provides important information about the nature of the one-way expansion, but also correctly models waves that travel close to the lateral direction. [40] derives the following approximate narrow-angle amplitude correction (or energy-flux normalization) terms

$$\mathbf{\Lambda}_1 = \mathbb{T} \approx \mathbf{T}_0 + \mathbf{T}_\alpha p_\alpha + \mathbf{T}_{\alpha\beta} p_\alpha p_\beta. \quad (64)$$

These approximate amplitude correction terms are evaluated by the following recursive equations

$$\mathbf{P}_0 \mathbf{T}_0 + \mathbf{T}_0 \mathbf{P}_0 = i \left(\mathbf{M}_0^\dagger \mathbf{P}_0 - \mathbf{P}_0 \mathbf{M}_0^\dagger + \partial_3 \mathbf{P}_0 \right),$$

$$\begin{aligned}
\mathbf{P}_0 \mathbf{T}_\alpha + \mathbf{T}_\alpha \mathbf{P}_0 &= \mathbf{T}_0 \mathbf{A}_\alpha^\dagger - \mathbf{A}_\alpha^\dagger \mathbf{T}_0 - \mathbf{P}_\alpha \mathbf{T}_0 - \mathbf{T}_0 \mathbf{P}_\alpha + \\
&\quad i \left(\mathbf{Q}_\alpha^\dagger + \mathbf{M}_0^\dagger \mathbf{P}_\alpha - \mathbf{P}_\alpha \mathbf{M}_0^\dagger + \right. \\
&\quad \left. \mathbf{M}_0^\dagger \mathbf{A}_\alpha^\dagger - \mathbf{A}_\alpha^\dagger \mathbf{M}_0^\dagger + \partial_3 \mathbf{A}_\alpha^\dagger + \partial_3 \mathbf{P}_\alpha \right) , \\
\mathbf{P}_0 \mathbf{T}_{\alpha\beta} + \mathbf{T}_{\alpha\beta} \mathbf{P}_0 &= \mathbf{T}_\alpha \mathbf{A}_\beta^\dagger - \mathbf{A}_\beta^\dagger \mathbf{T}_\alpha - \mathbf{P}_\alpha \mathbf{T}_\beta - \mathbf{T}_\alpha \mathbf{P}_\beta - \mathbf{P}_{\alpha\beta} \mathbf{T}_0 - \mathbf{T}_0 \mathbf{P}_{\alpha\beta} \\
&\quad + i \left(\mathbf{M}_0^\dagger \mathbf{P}_{\alpha\beta} - \mathbf{P}_{\alpha\beta} \mathbf{M}_0^\dagger + \partial_3 \mathbf{P}_{\alpha\beta} \right) , \tag{65}
\end{aligned}$$

where $\mathbf{M}_0^\dagger = (1/2)\mathbf{C}_{33}^{-1}\partial_3\mathbf{C}_{33}$, $\mathbf{A}_\alpha^\dagger = (1/2)\mathbf{C}_{33}^{-1}(\mathbf{C}_{\alpha 3} + \mathbf{C}_{3\alpha})$ and $\mathbf{Q}_\alpha^\dagger = \mathbf{C}_{33}^{-1}\partial_3\mathbf{C}_{33} - (1/2)\partial_3\mathbf{C}_{33}^{-1}(\mathbf{C}_{\alpha 3} + \mathbf{C}_{3\alpha})$. The amplitude correction matrices of equation (65) are complex valued, functions of both the medium elasticity and the subpropagator matrices, and evaluated in the same manner as equations (59)–(61).

Including the higher order amplitude correction terms of equation (65) in the approximation of the operator-root, $\mathbf{\Lambda}$, the true amplitude frequency domain narrow-angle wave equation is written

$$\begin{aligned}
\partial_1 \mathbf{u} &= \left[i\omega \left(\mathbf{P}_0 + \frac{1}{\omega} \mathbf{T}_0 - \frac{1}{i\omega} \mathbf{M}_0^\dagger \right) + \left(\mathbf{P}_\alpha + \frac{1}{\omega} \mathbf{T}_\alpha \right) \partial_\alpha \right. \\
&\quad \left. + \frac{1}{i\omega} \left(\mathbf{P}_{\alpha\beta} + \frac{1}{\omega} \mathbf{T}_{\alpha\beta} \right) \partial_\alpha \partial_\beta \right] \mathbf{u} . \tag{66}
\end{aligned}$$

Comparing equation (66) with the leading-order narrow-angle wave equation (62), it can be seen that the amplitude correction matrices are indeed included as higher order terms in inverse frequency (ω^{-1}).

An intuitive understanding of the amplitude correction matrices of equation (65) can be found by inspecting their form in the isotropic, homogeneous limit. By restricting propagation to normal incidence, $p_\alpha = 0$, \mathbf{P}_0 reduces to a diagonal matrix of the inverse wavespeeds and the narrow-angle amplitude correction term given by equation (64) simplifies to

$$\mathbf{T} \approx \mathbf{T}_0 = \frac{1}{2} \frac{\partial_1 \mathbf{P}}{\mathbf{P}} . \tag{67}$$

The term $i\mathbf{T}_0 - \mathbf{M}_0$ represents the energy-flux normalization term (or differential transmission coefficient), which includes the effect of elasticity and density gradients in the x_3 direction. Since \mathbf{P}_α describes P -to- S wave coupling, \mathbf{T}_α represents an amplitude correction associated with P -to- S wave coupling from gradients. $\mathbf{T}_{\alpha\beta}$ appears to describe the effect material gradients have on wavefront curvature.

3.3.2 Acoustic heterogeneous case

Wide-angle Fourier or dual-domain derivations of one-way wave extrapolators, such as the phase-screen and wide-angle exponential propagator methods, represent a class of simulation algorithms that can efficiently calculate accurate

Greens functions in 3D heterogeneous media. The wide-angle one-way wave equation for 3D acoustic media [41] is written

$$\phi(x_1 + \epsilon, x_\alpha, p_\alpha; \omega) = \exp[i\omega P_1 \epsilon](1 + Q\epsilon)\phi(x_1, x_\alpha, p_\alpha; \omega), \quad (68)$$

where ϕ is the acoustic wavefield and ϵ is the incremental extrapolation step length in the x_1 direction. The phase propagator coefficient is defined

$$P_1(x_1, x_\alpha, p_\alpha) = \left[\frac{1}{v^2(x_1, x_\alpha)} - p_\alpha^2 \right]^{1/2}, \quad (69)$$

where $v(x_1, x_\alpha)$ is the 3D variable acoustic velocity. The propagator P_1 is the local x_1 component of slowness and serves to advance each plane-wave component of the acoustic wavefield in the preferred direction of propagation x_1 . The differential transmission coefficient is written

$$Q(x_1, x_\alpha, p_\alpha) = -\frac{1}{2} \frac{\partial_1 P_1}{P_1}. \quad (70)$$

The transmission coefficient is an energy-flux normalization (i.e., amplitude correction) term and becomes important when gradients in acoustic velocity in the propagation direction x_1 are significant [note that equation (70) is the acoustic equivalent to equation (67)]. The propagator and transmission coefficient terms are evaluated on the plane $x_1 + \epsilon/2$. Equation (68) has been shown to accurately simulate both the phases and amplitudes of the acoustic wavefield in 3D heterogeneous media [41]. [72] address some of the limitations of equation (68) when large material gradients exist in the velocity model, but for the examples presented in this paper the wide-angle wave extrapolator should provide accurate solutions.

Although these techniques can be considered computationally efficient methods when compared to more complete full-waveform methods, such as FD methods, they can still be computationally cumbersome, especially for 3D media. One of the significant computational costs of these algorithms stems from the shuttling between the space and wave number domains; for many algorithms, this shuttling is done via very efficient fast Fourier transforms (FFTs). Thus, improvements can be made by implementing theoretical approximations [73] or by manipulating model parameterization [41].

For each extrapolation step ϵ in the x_1 direction, the solution to equation (68) requires (i) one FFT to transform the wavefield ϕ from the lateral space domain x_α into the lateral wave number (or slowness) domain p_α and (ii) time consuming construction of the propagator $P_1(x_1, x_\alpha, p_\alpha)$ and transmission $Q(x_1, x_\alpha, p_\alpha)$ coefficient terms and an inverse FFT for each lateral grid point x_α to reconstruct the total wavefield from plane-wave components. [41] shows that a reduction in computational time can be obtained by implementing natural interpolation (i.e., interpolating the slowly varying amplitude terms P_1 and Q). [74] generalize the phase-shift (i.e., stationary exponential extrapolator) method to laterally varying media by introducing wavefield interpolation. In this method, lateral

velocity variations can be incorporated by interpolating wavefields extrapolated using the stationary phase–shift method using at least two reference velocities. The choice of the number of reference velocities is based on discretizing the velocity field such that the velocity increment (or step) never exceeds 50% and hence minimizing dispersion (or phase) error.

To simplify implementation of the wide–angle wave equation (68) and make use of the natural interpolation concept, we can introduce an automated linear interpolation scheme [42]. In this approach, at each $x_1 + \epsilon/2$ plane the acoustic velocity model is discretized into $i = (1, N)$ lateral velocities

$$V_{min}(x_1 + \epsilon/2, x_\alpha) \leq V^i \leq V_{max}(x_1 + \epsilon/2, x_\alpha) , \quad (71)$$

where V_{min} and V_{max} are the minimum and maximum model acoustic velocities, respectively. Next the propagator P_1 and transmission coefficient Q are evaluated for each discrete lateral velocity V_i . Then N acoustic wavefields $\phi^i(x_1 + \epsilon; \omega)$ are evaluated for each discrete lateral velocity V^i using the wide–angle equation (68). Finally, for each lateral x_α grid point, the complete wavefield $\phi(x_1 + \epsilon, x_\alpha, p_\alpha; \omega)$ is synthesized using the linear velocity interpolation scheme

$$\phi(x_1 + \epsilon, x_\alpha, p_\alpha; \omega) = \eta \phi^i(x_1 + \epsilon; \omega) + (1 - \eta) \phi^{i+1}(x_1 + \epsilon; \omega) , \quad (72)$$

when $V^i \leq V(x_1, x_\alpha) \leq V^{i+1}$. The linear scaling factor is

$$\eta = \left[1 - \frac{V(x_1, x_\alpha) - V^i}{\Delta V} \right] , \quad (73)$$

where

$$\Delta V = \left[\frac{V_{min}(x_1 + \epsilon/2, x_\alpha) - V_{max}(x_1 + \epsilon/2, x_\alpha)}{(N - 1)} \right] . \quad (74)$$

4 Numerical examples

Anisotropy and heterogeneity in the Earth exists on a variety of scales, ranging from several tens of kilometres down to meters in tectonic settings, meters to centimetres in exploration and engineering applications, and down to less than millimetres in hand sample specimens. As well, in many applications, significant fine scale anisotropic fabric in the form of crystalline or lattice–preferred orientation, and/or shape–preferred orientation (SPO), such as horizontal alignment of micaceous minerals in shales, can be observed. Since the frequency content of the probing seismic energy (i.e., the relative scale lengths involved) dictates how the wave interacts with the medium, a heterogeneous medium may appear either very simple producing predictable wave phenomena or extremely complex generating incoherent waveform distortion and attenuation [39]. Furthermore, variations in orientation and averaging of fine scale anisotropic fabric make its net effect on longer wavelength seismic signals difficult to access. As well, when

anisotropic fabric is coherent and has significant strength, frequency-dependent waveform and wavefront distortion arise from slowness surface indentations (i.e., wavefront folding) as well as slowness surface intersections (or singularities), where rapid rotations and discontinuities in wave mode polarisations lead to a strong frequency-dependent coupling or leakage between quasi-shear waves in a gradient [37].

With improvements in data quantity and quality, improved waveform simulation using algorithms based on physically-motivated approximations that describe the frequency-dependent effects of wave propagation are becoming increasingly important [75; 76]. For instance, in the pioneering study of [77], the acoustic parabolic equation of [78] was adapted to study the P-wave travel-time and amplitude anomalies over the NORSAR array. Their results indicated that the 3D heterogeneities in the underlying lithosphere/asthenosphere could be modeled, that the observed large scale traveltime and amplitude anomalies across the array share the same structural origin, and that the teleseismic P-waves are deflected no more than 5° from the propagation path. The narrow-angle propagator not only has the ability to model such 3D heterogeneity, but it also has the ability to augment interpretation by considering anisotropic slowness surface and polarization effects as well as utilizing the entire three-component waveform [75].

In this section I show waveform modeling results using the one-way wave equations applied to various applications. The results will highlight the key feature of the one-way wave equation approach by stressing its ability to model gradual vector waveform evolution along the underlying wavefront. Specifically, the results will show that the one-way wave equation is capable of modeling the evolution of important and observable wave phenomena across an array, and so can help in constraining not only the vertical, but also the lateral variations in material properties.

4.1 Global applications: shear-wave splitting

Seismic anisotropy in the upper mantle is a commonly observed seismic phenomenon. Shear-wave splitting analysis (e.g., from SKS phases) has become the standard tool in assessing seismic anisotropy to infer fabric and tectonic evolution. This is because shear-wave splitting provides the most unambiguous measure of anisotropy. Large lateral variations in measured splitting parameters are often observed over small spatial distances due to tectonic features. Constraining the depth extent of observed seismic anisotropy can be difficult, but, if possible, can help distinguish the lithospheric and the asthenospheric components of anisotropy.

To gain insight into the tectonic evolution of the Main Ethiopian Rift, [75] investigated the feasibility of using shear wave splitting analysis and waveform modeling to constrain spatial variations in anisotropy. To do this, they used the narrow-angle wave equation (62) to simulate bandlimited waveforms for a suite of models. The models represented regions with rapidly changing anisotropy not too dissimilar to the Main Ethiopian Rift. [75] showed that variation in shear-

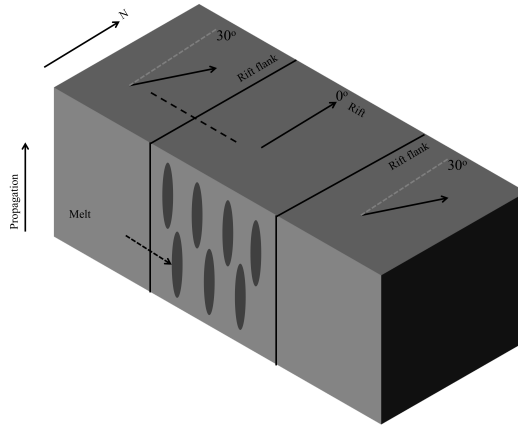


Figure 2: Schematic representation of the Ethiopian rift. The dashed line along the border of the Eastern rift border represents the subset of waveforms shown in the following figures.

wave splitting delay, δt , is dependent on source frequency, initial polarization as well as the vertical thickness of the anisotropic medium.

In Figures 3–5, I show some new results from this study to highlight the strength of using bandlimited waveform modeling to help constrain hypotheses. This is important because there is often some confusion regarding the non-uniqueness of seismic forward modeling versus seismic inversion. For instance, [79] states:

Others attempt to explain their results using forward modeling (e.g., Hammond et al., 2010a,b). However, forward modeling of SWS observations suffers from the problem of non-uniqueness and it does not fully explore the true extent of the parameter space. To get a quantitative parameterisation of the spatial distribution of anisotropy, SWS observations should be interpreted in tomographic inversion fashion.

However, this statement is very misleading and only true if the forward problem in the tomographic algorithm is solved exactly (i.e., exact Green’s function), and this is often not the case. Tomographic algorithms tend to use ray theoretical approximations and this is because it allows for efficient searches for the optimal model [e.g., 80]. However, if the wave physics is not modeled correctly then any quantitative parameterisation is likely to be inaccurate (or as good as the forward model used in the tomographic code). Thus, the implied statement that tomography suffers less from non-uniqueness is ill-informed. Ideally, the best approach is to let tomography guide the range of possible models to be tested with suitably advanced forward modeling algorithms.

For the global shear-wave modeling, [75] used a real SKS wavelet extracted from a typical SKS waveform from the Ethiopian seismic array. The propagated initial SKS wavefield had a backazimuth of 40° . The elastic anisotropic model

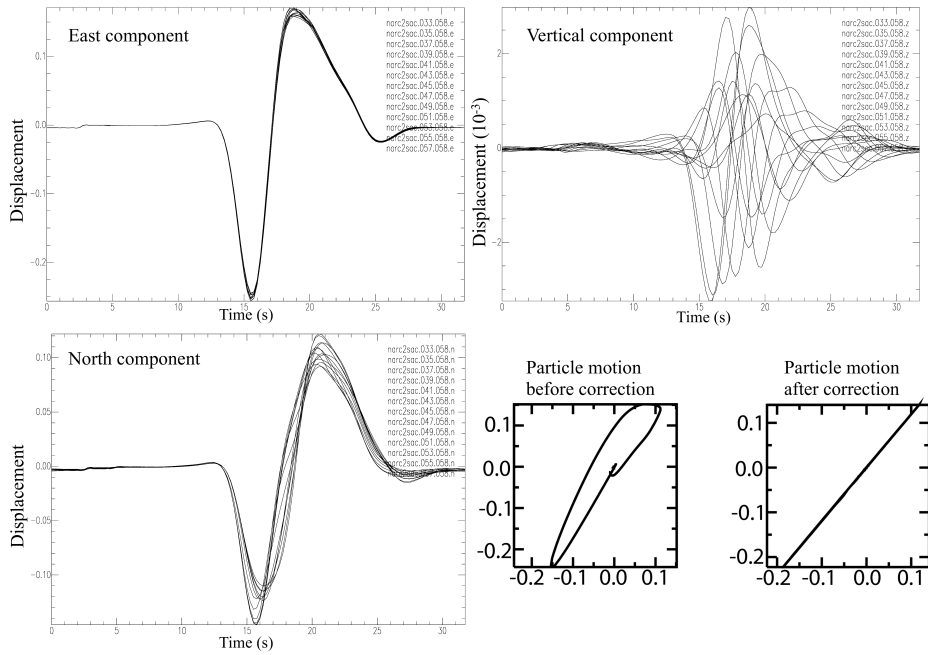


Figure 3: Synthetic waveforms propagated through the eastern margin of Ethiopian rift model (the model is symmetric). Shown are the displacement waveforms for the East, North and Vertical components (note that the waveforms for each component along the array are overlaid and that the amplitude of the Vertical component is orders of magnitude less than the East and North components). Also shown is a sample plot of the particle motion before and after shear wave splitting correction.

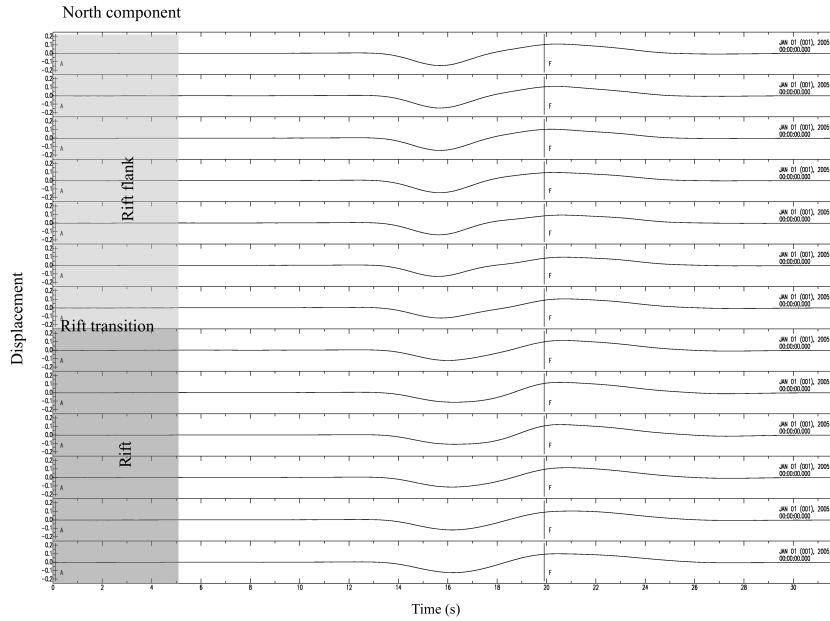


Figure 4: North component displacement waveforms of the propagated wavefield. The waveforms show very little variation across the rift transition.

had a depth of 45 km and total lateral extent of $300 \times 300 \text{ km}^2$ with rift zone width of 100 km in the middle (see Figure 2). The strength of anisotropy was constant throughout the model at 10%, with fast direction of 30° outside the rift (i.e., on the flanks) and 0° within the rift. The initial polarization of the SKS shear-wave was 40° with a dominant period of 8 s. The elasticity was based on background P- and S-wave velocities of 7800 and 4000 km/s, and density of 3800 kg/m^3 . The anisotropy was modeled as aligned cracks [81] with crack infill P- and S-wave velocities of 2500 and 0 km/s, and density of 2700 kg/m^3 . The cracks were modeled as penny-shaped inclusions with an aspect ratio of 0.01.

Figure 3 shows the synthetic displacement waveforms for all three components along the sub-array shown in Figure 2. The East component displacement waveforms are relatively constant, whereas there is observable variation in the North component displacement waveforms. Although the magnitude of the Vertical component displacement waveforms are several orders of magnitude less than the horizontal components, they show significant variation across the array. In Figure 4, the North component of displacement is shown across the sub-array. Visually the subtle variations in waveforms seen in Figure 3 are indistinguishable. However, inspecting Figure 5, it can be seen that the Vertical component waveform variations are strong and physically meaningful. This variation results from frequency-dependent shear-wave coupling resulting from the rotation of the anisotropic elastic tensor across the rift [e.g., 37; 76].

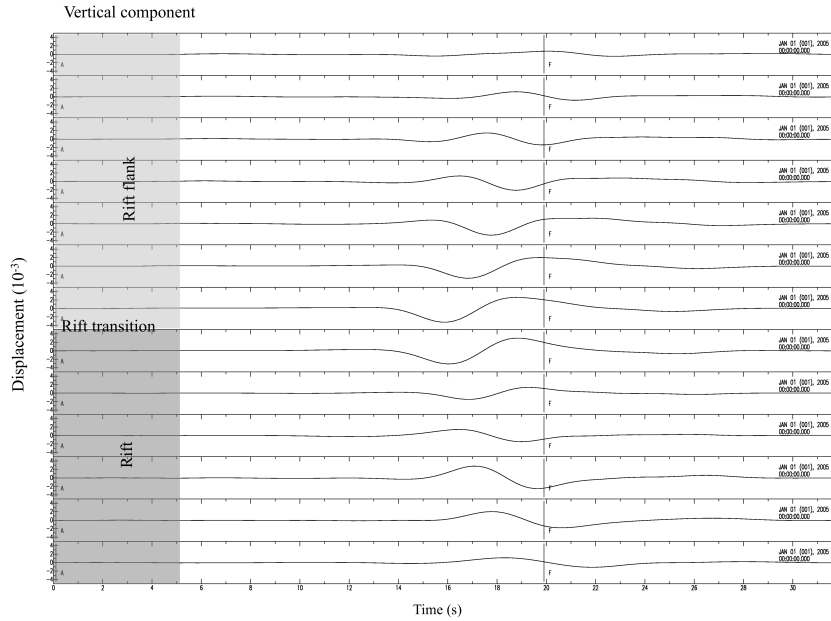


Figure 5: Vertical component displacement waveforms of the propagated wavefield. The waveforms show the influence of shear-wave coupling due to the rotation of the shear-wave fast-axis across the transition.

Based on varying key model parameters and performing several simulations, [75] were able to estimate the region of anisotropy in the Ethiopian Rift that extends to an approximate depth of 90 km, beneath both flanks and the rift. Along the margins, anisotropy was estimated to have fast-axis orientation of 30° , whereas the rift valley was estimated to be orientated at 0° . By using the modeling results, the measured variation in δt of the observed seismic data could be attributed to the influence of the two different anisotropic regimes on the seismic wavefield.

4.2 Exploration applications: frequency dependent shear-wave splitting

Imaging fractures and fracture systems within hydrocarbon reservoirs has been of great interests over the past few decades. Although the relationship between reservoir permeability and fractures is complex, it is recognized that fractures play an important role in reservoir fluid flow. The compliance of fractures influences the deformation behaviour and hence influences the fluid pathways within fractures. Although field-scale seismic techniques do not have sufficient resolution to image individual fractures, the presence of fracture systems can be observed and characterised via seismic anisotropy. Seismic anisotropy in reser-

voirs can be due not only to preferred alignment of sub-seismic scale fractures, but also due to intrinsic anisotropy, fine-scale layering or fabric and the influence of non-hydrostatic changes in the stress field on microcracks and grain boundaries [82]. The fact that sub-seismic scale fractures can lead to anisotropy is because fractures form coherent regions with directional dependence of reduced strength. There are several techniques to measure seismic anisotropy that can estimate fracture orientation and strength, such as Amplitude Versus Offset and Azimuth (AVOA). However, distinguishing between the various sources of seismic anisotropy as well as seismic heterogeneity is often not a simple task [e.g., 83; 84], and interpretation can be complicated further by frequency-dependent anisotropy [85].

Measurement of fracture compliance from static and dynamic measurement can provide valuable information on fracture strength and potential fracture infill [86; 87; 88]. [88] use the excess compliance formulation of [89] to map P-wave anisotropy measurements to excess fracture compliance. As well, theoretical predictions [90; 91] and ultrasonic observations [92] have shown that the ratio of normal to tangential compliance may be an indicator of fluid fracture content. However, it is difficult to uniquely determine from seismic data whether a fracture set is composed of a few large compliant fractures, or a larger number of small stiff fractures. Several recent investigations have reported frequency-dependent anisotropy within hydrocarbon reservoirs, such that the measured anisotropy decreases with increasing frequency [85; 93; 94; 95]. Assuming seismic anisotropy is due to aligned fractures and their compliance, a mechanism that reduces the apparent compliance of the fractures with increasing frequency is required. Two possible mechanisms to achieve this are (i) wave induced fluid flow between fractures and pores and (ii) scattering due to rough fractures.

The presence of fluid within fractures can significantly reduce its normal compliance. Assuming the background rock matrix is porous and permeable, the response of the fluid-filled fracture is dependent on the frequency of the seismic wave. For low frequencies, the fluid pressure can equilibrate (i.e., the fluid has time to flow out of the fractures) in response to the seismic disturbance and hence the effect of fluid on fracture compliance is minimal. However, at high frequencies, the wave disturbance may be too rapid for the fractures to fully drain and hence the fractures will appear stiff. [96] developed a poroelastic squirt-flow model, where the frequency dependence is strongly influenced by the porosity and permeability of the host rock, the fluid properties (e.g., viscosity and bulk modulus) and the average size of the fractures (with larger fractures affecting lower frequencies). [97] measured frequency dependent fracture compliance in lab samples and demonstrated that the frequency dependence could be due to waveform scattering as the wave propagates through a non-uniform distribution of local compliance within the plane of a rough fracture. [98] generalize the results of [96] and [97] and propose a method to model the frequency dependent anisotropy due to scattering from aligned fluid-filled rough fractures. These results show a dependence on the mean compliance of the constituent fractures and can be used potentially to distinguish between anisotropy produced by large or small fractures.

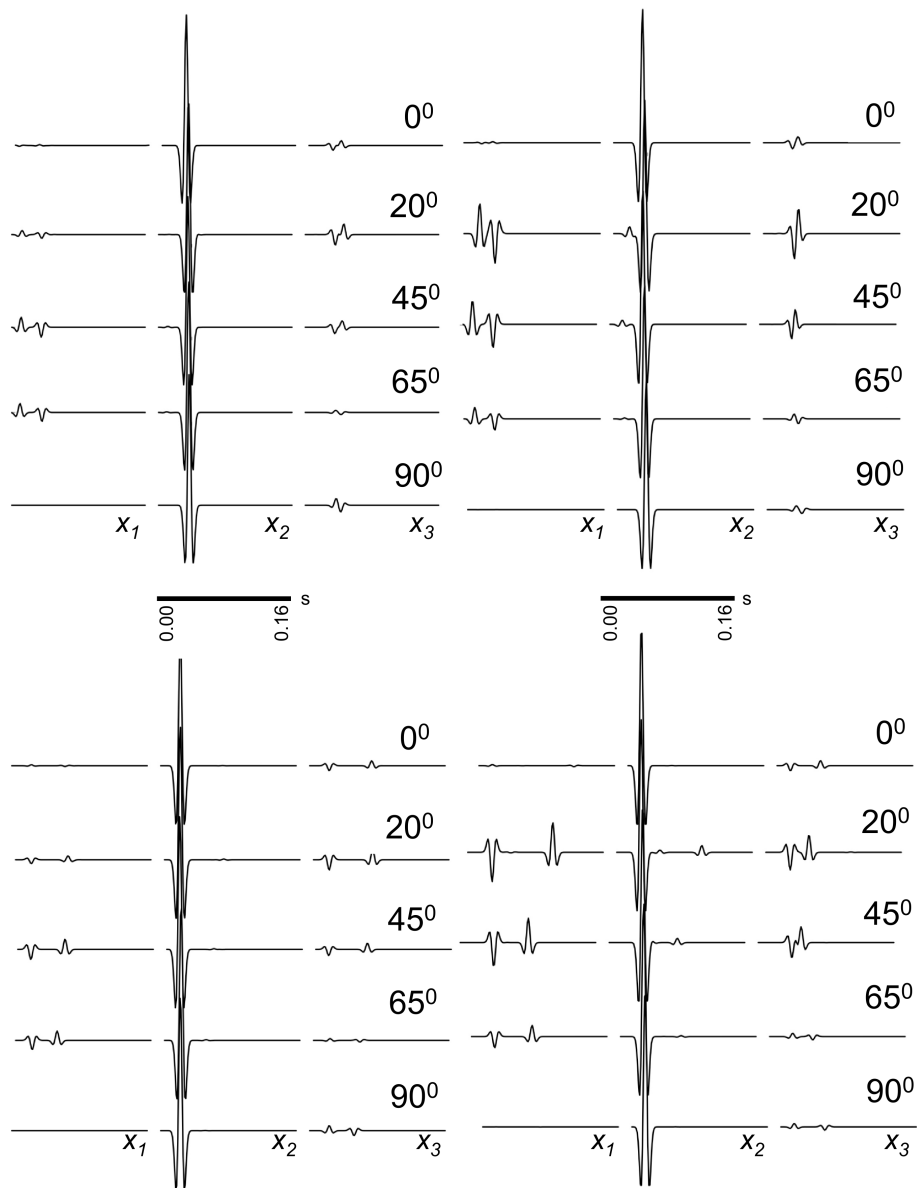


Figure 6: Propagated incident plane S-wave synthetic showing three components based on the [99] model on left and [100] model on right. The top panel is for a 80 Hz dominant frequency wavelet and bottom panel for a 400 Hz dominant wavelet. In each panel, the direction of horizontal propagation with respect to the fracture plane is 0° , 20° , 45° , 65° and 90° from top to bottom.

Here, I examine various waveform distortion effects for seismic wave propagation in fractured and porous media. Specifically, I consider two categories of effective medium fracture models: frequency independent media and frequency dependent media. Although the approach typically taken to model fractures in reservoirs is to assume frequency independence, recent evidence suggests frequency-dependent anisotropy and attenuation effects [e.g., 85]. For the first category (i.e., the frequency-independent effective media models), I use laboratory-derived elasticities of siliciclastic sandstones from the Clair reservoir, where grain-scale contributions to anisotropy are assessed using additional elastic compliances due to inter-granular effects [101]. The effect of fractures is modeled using the effective medium models of [99] and [100], and the effect of fluid is modeled using Gassman’s theory [102]. For the second category, the effect of fractures is simulated using the frequency-dependent fracture model of [98]. In the models of [96] and [98], the elasticity tensors are complex valued. Given that one form of the narrow-angle equation is expressed in the frequency domain (equation 62), these rock physics models can be implemented easily, leading to complex valued propagator matrices (equations 59–61 and 65).

In Figure 6, the results of propagating a shear-wave within the two different fracture models is shown. The models both assume a background vertical transverse isotropy (VTI) observed in the sandstones from the Clair reservoir [101]. In both fracture models, the crack density is 0.05 and aspect ratio of 0.05, and the permeability is 3 mD. For both fracture models, two source frequencies of 80 Hz and 400 Hz were used and five different horizontal propagation directions were simulated: 0° , 20° , 45° , 65° and 90° to the fracture plane. The wavefield was propagated for a total distance of 200 m in the homogeneous anisotropic model. For directions normal (0°) and parallel (90°) to the fractures, there is minimal shear-wave splitting (i.e., there is no energy on the x_1 component). However, there is some energy on the x_3 component due to the lithological (VTI) anisotropy. For oblique angles of propagation, the shear-wave splitting is observable. The magnitude of the shear-wave splitting differs between the two fracture models, but the delay time and polarity are consistent. For the two source frequencies, the shear-wave splitting is the same (note the time axes are different) and hence there is no development of frequency-dependent anisotropy. The frequency dependence would only arise if the wave was propagating along the direction of a slowness singularity, where frequency-dependent shear-wave coupling would occur [e.g., 37].

In Figure 7, the results of propagating an incident shear-wave (initially a smoothly curved wavefront) within the frequency-dependent fracture models is shown. In this model, a background medium with isotropic P- and S-wave velocities of 4850 and 3200 m/s, respectively, density of 2110 kg/m^3 , and Thomsen parameters [103] $\epsilon = 0.24$, $\gamma = 0.11$ and $\delta = 0.20$ are used to generate the background VTI medium. The influence of fluid squirt-flow is modeled according to [96], with porosity $\phi = 10\%$, fluid bulk modulus $k_f = 0.0068e^9$, fracture flow relaxation parameter $\tau = 9.50e^{-7}$, and fracture density and aspect ratio of 0.024 and 1.0, respectively. After propagating 135 m and 270 m, the incident shear-wave with initial polarization primarily in the x_2 direction has split into a

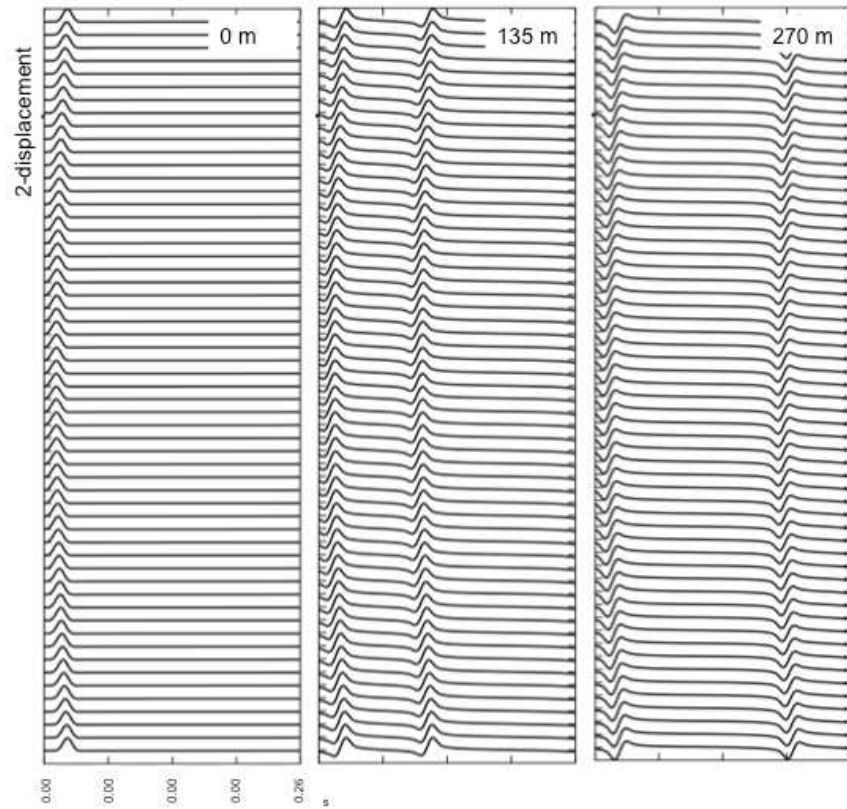


Figure 7: The x_2 component of the propagated incident curved S-wave withing the frequency-dependent fracture model at propagation distances of 0, 135 and 270 m.

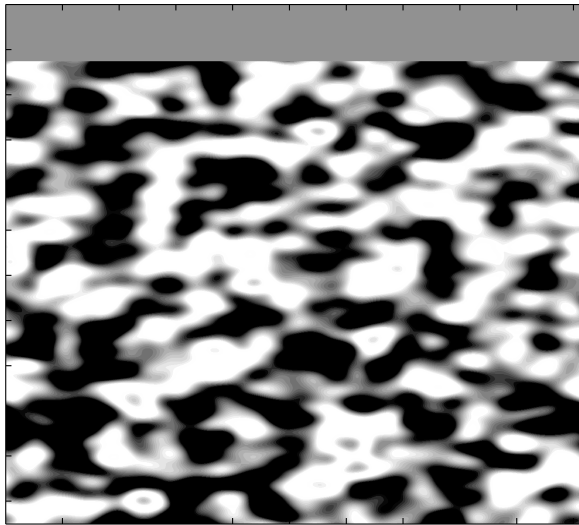


Figure 8: Random acoustic velocity model with background velocity of 3000 m/s and constant density of 2500 kg/m^3 . The medium has correlation length $a_1 = 30 \text{ m}$ in the depth (x_1) direction, $a_2 = 90 \text{ m}$ in the offset (x_2) direction and is invariant in the x_3 direction.

fast and slow component. As well, the effects of dispersion due to wave induced squirt-flow can be seen in the waveforms.

4.3 Acoustic applications: sub-Fresnel zone heterogeneity

To explore the efficiency and accuracy of implementing an automated linear acoustic velocity interpolation scheme, examples are presented for a 2D stochastic velocity model (see Figure 8). The acoustic velocity model is defined by anisotropic random Gaussian distributed heterogeneities, having correlation lengths of 90 m laterally (in the x_2 direction) and 30 m vertically (or in the x_1 direction) and a background velocity of 3000 m/s (the maximum velocity perturbation is on the order of $\pm 10\%$). The model is extended into 3D by introducing a third dimension (i.e., x_3) and is invariant with respect to x_2 . The random model has dimension $2048 \times 2048 \text{ m}^2$ laterally (x_α) and 1150 m vertically (x_1). For the examples presented, a plane-wave is extrapolated on a computational domain having 128×128 lateral grid points with 16 m spacing and x_1 extrapolation step ϵ of 2 m.

Figure 9 compares extrapolated plane-waves having a Ricker source wavelet with peak frequency of approximately 440 Hz. Although all simulations show similar wavefront distortion, it can be seen that as the number of velocity interpolants decrease so does the frequency content of the resulting waveforms (i.e., fewer high frequencies). Since the amplitudes between $N=8$ and 16 are comparable, the optimum number of model interpolants is likely close to $N=8$.

Figure 10 compares extrapolated plane-waves having a Ricker source wavelet with peak frequency of approximately 235 Hz. By lowering the source wavelet peak frequency, the effect of decreasing model interpolation on waveform frequency content is less pronounced. For this example, the optimum number of model interpolants is close to $N=4$.

The results indicate that the automated natural interpolation scheme allows sufficiently accurate computation of acoustic wavefields. For smoothly varying velocity models the scheme yields relatively identical results for both $N=2$ and 10 interpolants, even for large velocity perturbation [42]. The simulations indicate that there exists a trade-off between waveform frequency content and the number of model velocity interpolants. This suggests that when the medium is expected to vary significantly on the sub-Fresnel zone scale more interpolants are necessary to accurately simulate high frequencies. However, it should be stressed that the waveforms presented here were chosen deliberately in the high frequency range to enhance simulated wavefront and waveform distortion effects and to examine the limitations of the method for high frequency wavefields.

5 Conclusions

The one-way wave equation approach has been shown to accurately simulate the propagation of elastic waves in generally-anisotropic (for the elastic case) and smoothly varying heterogeneous, 3D media. Since the one-way propagator can be implemented in the frequency domain, I have shown also the potential of modeling wave propagation in visco-elastic media, such as the case of frequency-dependent fractured media. Although the vector elastic narrow-angle wave equation is the most restrictive of all the elastic one-way wave equations derived by [36], it does allow the closest examination of the influence of the elasticity tensor on wave propagation in terms of the local directional properties of the slowness surface and polarizations. Furthermore, adaptation to curvilinear coordinates can improve the narrow-angle restriction [38], increasing the range of allowable slownesses as well as introducing point-sources. A key feature of the one-way approach is the ability to model gradual vector (for the narrow-angle equations) and scalar (for the acoustic wide-angle equation) waveform evolution along the underlying wavefront. This is important because the Earth displays not only vertical, but also lateral variations in heterogeneity and anisotropy. Across a dense array of receivers, the gradual evolution of the seismic wavefield is observable and the variations in the frequency dependent effects due to anisotropy and heterogeneity can be significant. The capability of modeling the evolution of these wave phenomena across an array can not only help in constraining both the vertical and lateral variations in material properties, but also highlight significant observable wave phenomena. Thus, it is expected that the one-way propagator approach will be useful for a range of transmitted wave 3D global, exploration and engineering scale applications.

Although parallels can be drawn between the vector narrow-angle matrix formulation and conventional ray-based approaches, the narrow-angle wavefield

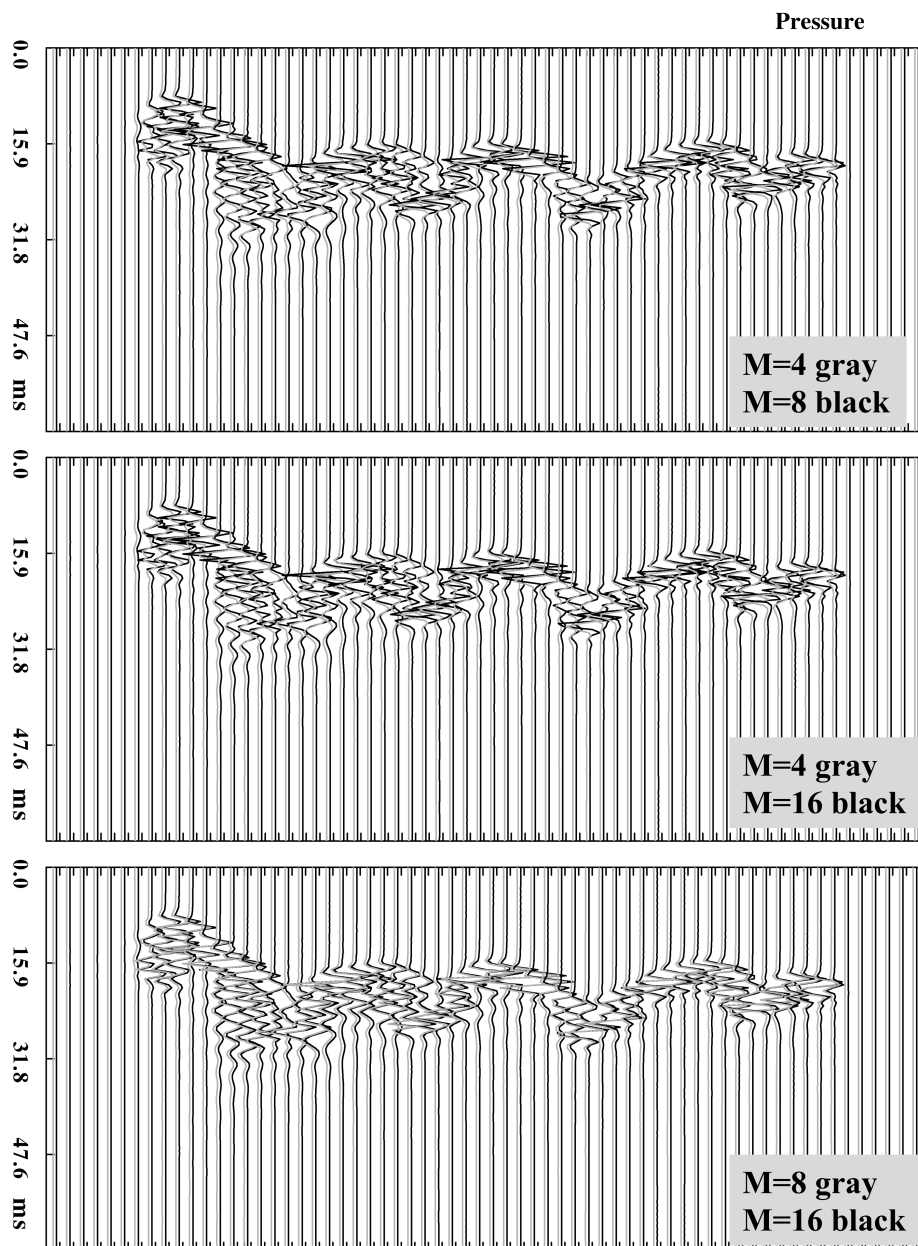


Figure 9: Extrapolated wavefields in random 2D acoustic velocity model for an input Ricker wavelet having peak frequency of 440 Hz. Waveforms are compared for various velocity interpolants (M). Simulations for all model interpolations show similar wavefront distortion, but the waveform frequency content varies, with the most noticeable difference being between $M = 4$ and $M = 16$ interpolants.

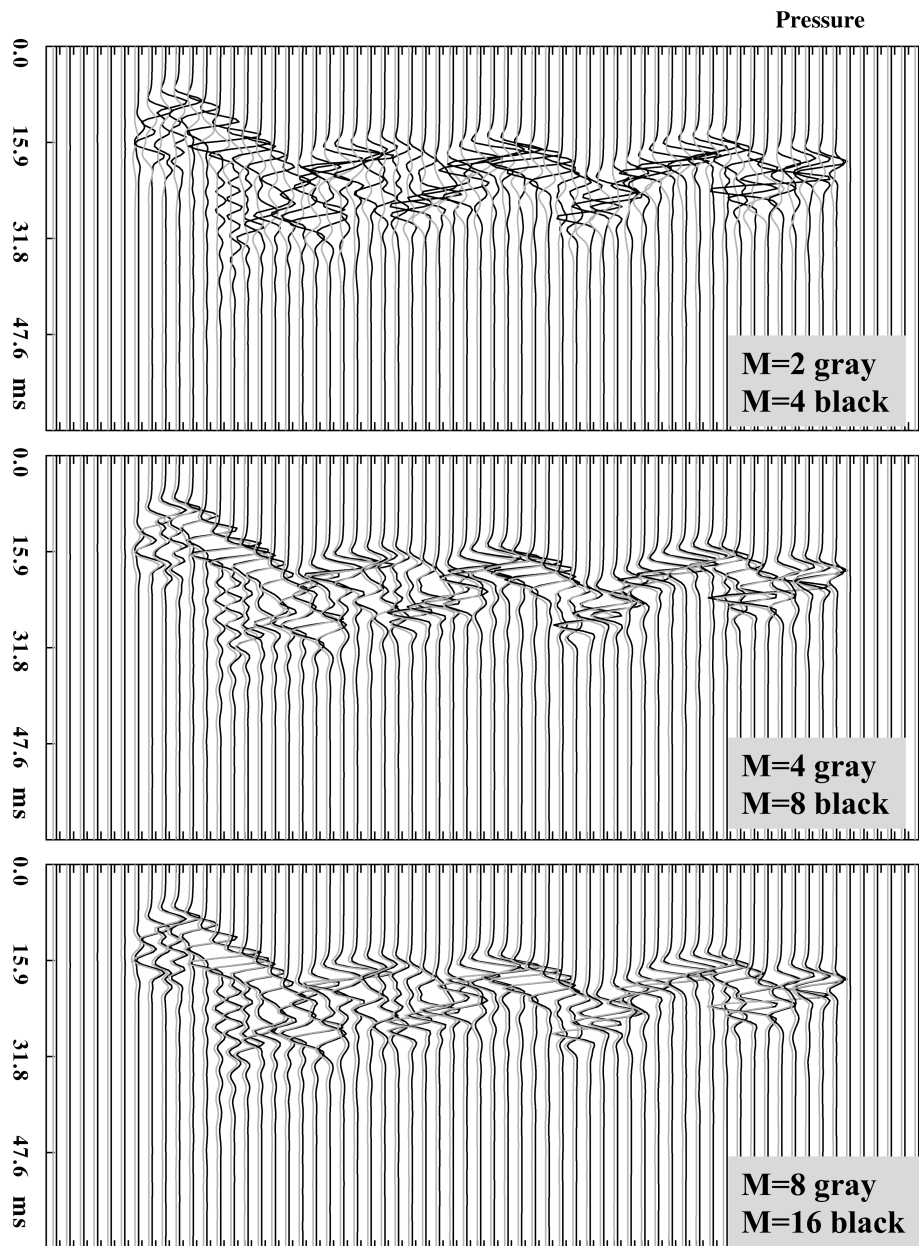


Figure 10: Extrapolated wavefields in random 2D acoustic velocity model for an input Ricker wavelet having peak frequency of 234 Hz. Waveforms are compared for various velocity interpolants (M). Simulations for all model interpolations show similar wavefront distortion and there appears to be an improvement between $M = 4$ and $M = 8$ velocity interpolants in comparison to the wavefield extrapolation at 440 Hz.

extrapolator is more generally applicable than ray methods. This is primarily because it can handle robustly transitions from weak-to-strong or arbitrary anisotropy, is not limited by caustics and can model wave coupling. However, it is important to reiterate that for most problems considered in seismology, there is no one correct approach to the evaluation of the wave solution. Rather, there are various approaches available and their appropriateness depends on the required accuracy, speed and robustness of the calculated solution.

In the opinion of [104], recent advances in computer architecture will allow 3D simulations of global seismic wave propagation on high-performance computing systems in a matter of seconds in the not so distant future. These computational advances will lead to earthquake source and tomographic inversions based solely on full-wave numerical methods, such as the spectral-element method [4; 105; 106]. Whether or not this view is overly optimistic, there is presently still a need for efficient, although approximate, wave solutions to constrain hypotheses. Furthermore, algorithms that are not restricted to parallel computing architectures, but rather can be performed on standard desktop computers will likely still be preferred, especially for researchers with limited computational resources. It is also possible that the one-way approach will be used in the field as a preliminary modeling or processing tool.

One of the primary difficulties associated with waveform inversion is the strong non-linearity of the inverse problem. This non-linearity becomes important when the medium is complicated, but is further aggravated when the data include large-offset or wide-angle data [69]. Large offset transmitted wave data are becoming increasingly prevalent because it has been recognized that they are required to resolve lateral structure [107]. In fact, a recent survey of frequency-domain waveform inversion algorithms has indicated that large offset transmitted or refracted data are commonly applied in seismic tomographic imaging [107]. The non-linearity of the inversion can be improved by preconditioning the data as well as having a good starting model. These starting models are usually obtained from conventional traveltimes tomography and so are limited by the asymptotic ray approximation. However, newer methods such as the so-called strongly damped wave equation can be used to compute the first-arrival traveltimes [108] or one-way wave equations to compute the most energetic traveltimes and amplitudes [54]. In theory, the acoustic wide-angle wave equation should be applicable to acoustic full-waveform inversion (and the narrow-angle wave equation for elastic full-waveform inversion) either as a means of generating a starting model or as an approximate elastic wave extrapolator for the iterative forward and reverse propagation steps. However, the theoretical details of its implementation in waveform inversion have yet to be clarified.

Acknowledgments

I would like to thank James Hammond for providing the SKS synthetic seismograms for the Ethiopian rift model, Alan Baird for providing the algorithm to

compute the frequency-dependent fracture induced elastic tensors, and Tobias Müller for providing the stochastic heterogeneous acoustic model.

References

- [1] J. Carcione, G. Herman, and A. ten Kroode, “Y2K review article: Seismic modeling,” *Geophysics*, vol. 67, pp. 1304–1325, 2002.
- [2] Z. Alterman and F. Karal, “Propagation of elastic waves in layered media by finite difference methods,” *B.S.S.A.*, vol. 58, pp. 367–398, 1968.
- [3] K. Kelly, R. Ward, S. Treitel, and R. Alford, “Synthetic seismograms: a finite-difference approach,” *Geophysics*, vol. 41, pp. 2–27, 1976.
- [4] D. Komatitsch and J. Tromp, “Introduction to the spectral-element method for 3-D seismic wave propagation,” *Geophys. J. Int.*, vol. 139, pp. 806–822, 1999.
- [5] W. Smith, “The application of finite element analysis to body wave propagation problems,” *Geophys. J. R. astr. Soc.*, vol. 42, pp. 747–768, 1975.
- [6] D. Kosloff, R. Reshef, and D. Loewenthal, “Elastic wave calculations by the Fourier method,” *B.S.S.A.*, vol. 74, pp. 875–891, 1984.
- [7] S.-H. Hung and D. Forsyth, “Modelling anisotropic wave propagation in oceanic inhomogeneous structures using the parallel multidomain pseudo-spectral method,” *Geophys. J. Int.*, vol. 133, pp. 726–740, 1998.
- [8] V. Červený, *Seismic Ray Theory*. Cambridge University Press, 2001.
- [9] R. Haddon and P. Buchen, “Use of Kirchhoffs formula for body wave calculations in the Earth,” *Geophys. J. R. astr. Soc.*, vol. 67, pp. 587–598, 1981.
- [10] L. Frazer and J. Sinton, “A Kirchhoff method for the computation of finite-frequency body wave synthetic seismograms in laterally inhomogeneous media,” *Geophys. J. R. astr. Soc.*, vol. 78, pp. 413–429, 1984.
- [11] C. Chapman, “Ray theory and its extensions: WKBJ and Maslov seismograms,” *J. Geophys.*, vol. 58, pp. 27–43, 1985.
- [12] J.-M. Kendall and C. Thomson, “Maslov ray summation, pseudocaustics, Lagrangian equivalence and transient seismic waveforms,” *Geophys. J. Int.*, vol. 113, pp. 186–214, 1993.
- [13] R. Nowack, “Calculation of synthetic seismograms with Gaussian beams,” *Pure Appl. Geophys.*, vol. 160, pp. 487–507, 2003.
- [14] C. Thomson, “Seismic coherent states and ray geometrical spreading,” *Geophys. J. Int.*, vol. 144, pp. 320–342, 2001.

- [15] B. Kennett, *Seismic Wave Propagation in Stratified Media*. Cambridge University Press, 1983.
- [16] J. Hudson and J. Heritage, “The use of the Born approximation in seismic scattering problems,” *Geophys. J. R. astr. Soc.*, vol. 66, pp. 221–240, 1981.
- [17] R.-S. Wu and M. Toksöz, “Diffraction tomography and multisource holography applied to seismic imaging,” *Geophysics*, vol. 52, no. 1, pp. 11–25, 1987.
- [18] M. Woodward, “Wave-equation tomography,” *Geophysics*, vol. 57, no. 1, pp. 15–26, 1992.
- [19] M. Panning, Y. Capdeville, and B. Romanowicz, “Seismic waveform modelling in a 3-D Earth using the Born approximation: potential shortcomings and a remedy,” *Geophys. J. Int.*, vol. 177, pp. 161–178, 2009.
- [20] A. Ishimaru, *Wave Propagation and Scattering in Random Media*, vol. 1 and 2. Academic Press, 1978.
- [21] J. Spetzler and R. Snieder, “The effect of small-scale heterogeneity on the arrival time of waves,” *Geophys. J. Int.*, vol. 145, pp. 786–796, 2001.
- [22] A. Lomax, “Path-summation waveforms,” *Geophys. J. Int.*, vol. 138, pp. 702–716, 1999.
- [23] R. Schlottmann, “A path integral formulation of acoustic wave propagation,” *Geophys. J. Int.*, vol. 137, pp. 353–363, 1999.
- [24] J. Claerbout, “Coarse grid calculations of wave in inhomogeneous media with application to delineation of complicated seismic structure,” *Geophysics*, vol. 35, no. 3, pp. 407–418, 1970.
- [25] F. Tappert and R. Hardin, “Computer simulation of long-range ocean acoustic propagation using the parabolic equation method,” in *Proc. 8th Intern. Cong. on Acoustics*, vol. 2, p. 452, Goldcrest, London, 1974.
- [26] L. Fishmann and J. McCoy, “Derivation and application of extended parabolic wave theories. I. The factorized Helmholtz equation,” *J. Math. Phys.*, vol. 25, pp. 285–296, 1984.
- [27] R.-S. Wu, “Wide-angle elastic wave one-way propagation in heterogeneous media and an elastic wave complex-screen method,” *J. Geophys. Res.*, vol. 99, pp. 751–766, 1994.
- [28] A. Wild and J. Hudson, “A geometrical approach to the elastic complex screen,” *J. Geophys. Res.*, vol. 103, pp. 707–725, 1998.
- [29] A. Haines, “A phase-front method, III, Acoustic waves, P- and S-waves,” *Geophys. J. R. astr. Soc.*, vol. 77, pp. 65–103, 1984.

- [30] J. le Rousseau and M. de Hoop, “Scalar generalized–screen algorithms in transversely isotropic media with a vertical symmetry axis,” *Geophysics*, vol. 66, no. 5, pp. 1538–1550, 2001.
- [31] F. Jensen, W. Kuperman, M. Porter, and H. Schmidt, *Computational Ocean Acoustics*. Modern Acoustics and Signal Processing, American Institute of Physics, 1994.
- [32] M. Levy, *Parabolic Equation Methods for Electromagnetic Wave Propagation*. IEE Electromagnetic Waves Series 45, The Institution of Electrical Engineers, London, 2000.
- [33] M. Leontovich and V. Fock, “Solution of the problem of propagation of electromagnetic waves along the Earth’s surface by the method of parabolic equation,” *Acad. Sci. USSR. J. Phys.*, vol. 10, pp. 13–24, 1946. Engl. transl.
- [34] R. Clayton and B. Engquist, “Absorbing boundary conditions for acoustic and elastic wave equations,” *B.S.S.A.*, vol. 67, no. 6, pp. 1529–1540, 1977.
- [35] L. Fishmann and J. McCoy, “A new class of propagation models based on a factorization of the Helmholtz equation,” *Geophys. J. R. astr. Soc.*, vol. 80, pp. 439–461, 1985.
- [36] C. Thomson, “The ‘gap’ between seismic ray theory and ‘full’ wavefield extrapolation,” *Geophys. J. Int.*, vol. 137, pp. 364–380, 1999.
- [37] D. Angus, C. Thomson, and R. Pratt, “A one–way wave equation for modelling seismic waveform variations due to elastic anisotropy,” *Geophys. J. Int.*, vol. 156, pp. 595–614, 2004.
- [38] D. Angus and C. Thomson, “Numerical analysis of a narrow–angle, one–way, elastic–wave equation and extension to curvilinear coordinates,” *Geophysics*, vol. 71, pp. T137–T146, 2006.
- [39] D. Angus, “A one–way wave equation for modelling seismic waveform variations due to elastic heterogeneity,” *Geophys. J. Int.*, vol. 162, pp. 882–898, 2005.
- [40] D. Angus, “True amplitude corrections for a narrow–angle one–way elastic wave equation,” *Geophysics*, vol. 72, pp. T19–T26, 2007.
- [41] C. Thomson, “Accuracy and efficiency considerations for wide–angle wavefield extrapolators and scattering operators,” *Geophys. J. Int.*, vol. 163, pp. 308–323, 2005.
- [42] D. Angus and J.-M. Kendall, “Improved computational efficiency of a 3–D wide–angle acoustic extrapolator via model interpolation,” *EAGE Expanded Abstracts, London, UK*, 2007.

- [43] J. Claerbout and A. Johnson, “Extrapolation of time-dependent waveforms along their path of propagation,” *Geophys. J. R. astr. Soc.*, vol. 26, pp. 285–293, 1971.
- [44] T. Landers and J. Claerbout, “Numerical calculations of elastic waves in laterally inhomogeneous media,” *J. Geophys. Res.*, vol. 77, no. 8, pp. 1476–1482, 1972.
- [45] J. Hudson, “A parabolic approximation for elastic waves,” *Wave Motion*, vol. 2, pp. 207–214, 1980.
- [46] J. Claerbout, *Imaging the Earth’s Interior*. Blackwell Scientific Publication, first ed., 1985.
- [47] J. Claerbout and S. Doherty, “Downward continuation of moveout-corrected seismograms,” *Geophysics*, vol. 37, no. 5, pp. 741–768, 1972.
- [48] J. Claerbout, *Imaging the Earth’s Interior*. Samizdat Press, second ed., 1996.
- [49] J. Scales, *Theory of Seismic Imaging*. Samizdat Press, 1994.
- [50] P. Hubral, “Time migration – some ray theoretical aspects,” *Geophys. Pros.*, vol. 25, pp. 738–745, 1977.
- [51] K. Larner, L. Hatton, B. Gibson, and I.-C. Hsu, “Depth migration of imaged time sections,” *Geophysics*, vol. 46, pp. 734–750, 1981.
- [52] L. Hatton, K. L. Larner, and B. S. Gibson, “Migration of seismic data from inhomogeneous media,” *Geophysics*, vol. 46, pp. 751–767, 1981.
- [53] M. Lee and S. Suh, “Optimization of one-way wave equations,” *Geophysics*, vol. 50, no. 10, pp. 1634–1637, 1985.
- [54] C. Shin, S. Ko, W. Kim, D.-J. Min, D. Yang, K. Marfurt, S. Shin, K. Yoon, and C. Yoon, “Travelttime calculations from frequency-domain downward-continuation algorithms,” *Geophysics*, vol. 68, no. 4, pp. 1380–1388, 2003.
- [55] M. Feit and J. Fleck, “Light propagation in graded-index optical fibers,” *Applied Optics*, vol. 17, no. 24, pp. 3990–3998, 1978.
- [56] D. Thomson and N. Chapman, “A wide-angle split-step algorithm for the parabolic equation,” *J. Acoust. Soc. Am.*, vol. 74, no. 6, pp. 1848–1854, 1983.
- [57] R. Greene, “A high-angle one-way wave equation for seismic wave propagation along rough and sloping interfaces,” *J. Acoust. Soc. Am.*, vol. 77, no. 6, pp. 1991–1998, 1985.
- [58] B. Wetton and G. Brooke, “One-way wave equations for seismoacoustic propagation in elastic waveguides,” *J. Acoust. Soc. Am.*, vol. 87, no. 2, pp. 624–632, 1990.

- [59] M. Collins, “A higher-order parabolic equation for wave propagation in an ocean overlying an elastic bottom,” *J. Acoust. Soc. Am.*, vol. 86, no. 4, pp. 1459–1464, 1989.
- [60] A. Bamberger, B. Enquist, L. Halpern, and P. Joly, “Higher order paraxial wave equation approximations in heterogeneous media,” *SIAM J. Appl. Math.*, vol. 48, no. 1, pp. 129–154, 1988.
- [61] M. Collins, “Higher-order Padé approximations for accurate and stable elastic parabolic equations with application to interface wave propagation,” *J. Acoust. Soc. Am.*, vol. 89, no. 3, pp. 1050–1057, 1991.
- [62] A. Fredricks, W. Siegmann, and M. Collins, “A parabolic equation for anisotropic elastic media,” *Wave Motion*, vol. 31, pp. 139–146, 2000.
- [63] M. de Hoop and A. de Hoop, “Elastic wave up/down decomposition in inhomogeneous and anisotropic media: an operator approach and its approximations,” *Wave Motion*, vol. 20, pp. 57–82, 1994.
- [64] J. Woodhouse, “Surface waves in a laterally varying layered structure,” *Geophys. J. R. astr. Soc.*, vol. 37, pp. 461–490, 1974.
- [65] M. de Hoop, “Generalization of the Bremmer coupling series,” *J. Math. Phys.*, vol. 37, no. 7, pp. 3246–3282, 1996.
- [66] M. de Hoop, J. L. Rousseau, and B. Biondi, “Symplectic structure of wave-equation imaging: a path-integral approach based on the double-square-root equation,” *Geophys. J. Int.*, vol. 153, pp. 52–74, 2003.
- [67] C. Chapman, “Long-period corrections to body waves: Theory,” *Geophys. J. R. astr. Soc.*, vol. 64, pp. 321–372, 1981.
- [68] M. van Stralen, M. de Hoop, and H. Blok, “Generalized Bremmer series with rational approximation for the scattering of waves in inhomogeneous media,” *J. Acoust. Soc. Am.*, vol. 104, no. 4, pp. 1943–1963, 1998.
- [69] L. Sirgue and R. Pratt, “Efficient waveform inversion and imaging: a strategy for selecting temporal frequencies,” *Geophysics*, vol. 69, no. 1, pp. 231–248, 2004.
- [70] J. Hudson, *The Excitation and Propagation of Elastic Waves*. Cambridge University Press, 1980.
- [71] Y. Egorov and B.-W. Schulze, *Pseudo-differential Operators, Singularities, Applications*, vol. 93 of *Operator theory: advances and applications*. Birkhäuser Verlag, 1991.
- [72] C. Thomson and C. Chapman, “True-amplitude wide-angle one-way propagators and high-gradient zones,” *EAGE 68th Conference and Exhibition, Expanded Abstracts*, p. H045, 2006.

- [73] R. Ferguson and G. Margrave, “Planned seismic imaging using explicit one-way operators,” *Geophysics*, vol. 70, pp. S101–S109, 2005.
- [74] J. Gazdag and P. Sguazzero, “Migration of seismic data by phase shift plus interpolation,” *Geophysics*, vol. 49, no. 2, pp. 124–131, 1984.
- [75] J. Hammond, J.-M. Kendall, D. Angus, and J. Wookey, “Interpreting spatial variations in anisotropy: insights into the Main Ethiopian Rift from SKS waveform modelling,” *Geophys. J. Int.*, vol. 181, pp. 1701–1712, 2010.
- [76] D. Angus and C. Thomson, “Modelling converted seismic waveforms in isotropic and anisotropic 1-D gradients: discontinuous versus continuous gradient representations,” *Studia Geophysica et Geodaetica*, vol. 56, no. 2, pp. 383–409, 2012.
- [77] R. Haddon and P. W. Buchen, “Use of Kirchhoff’s formula for body wave calculations in the Earth,” *Geophys. J. R. astr. Soc.*, vol. 67, pp. 587–598, 1981.
- [78] J. Claerbout, *Fundamentals of Geophysical Data Processing*. Blackwell Scientific Publications, 1976.
- [79] O. Al-Harrasi, *Fractured reservoir characterisation using shear-wave splitting in microseismic data: A case study from Oman*. PhD thesis, University of Bristol, 2010.
- [80] J. Wookey, “Direct probabilistic inversion of shear wave data for seismic anisotropy,” *Geophys. J. Int.*, vol. 189, no. 2, pp. 1025–1037, 2012.
- [81] J. Hudson, “Overall properties of a cracked solid,” *Math. Proc. Camb. Phil. Soc.*, vol. 88, pp. 371–384, 1980.
- [82] J. Verdon, D. Angus, J.-M. Kendall, and S. Hall, “The effect of microstructure and nonlinear stress on anisotropic seismic velocities,” *Geophysics*, vol. 73, pp. D41–D51, 2008.
- [83] J. Verdon and J.-M. Kendall, “Detection of multiple fracture sets using observations of shear-wave splitting in microseismic data,” *Geophys. Pros.*, vol. 59, no. 4, pp. 593–608, 2011.
- [84] A. Wuestefeld, J. Verdon, J.-M. Kendall, J. Rutledge, H. Clarke, and J. Wookey, “Inferring rock fracture evolution during reservoir stimulation from seismic anisotropy,” *Geophysics*, vol. 76, no. 6, pp. WC159–WC168, 2011.
- [85] S. Maultzsch, M. Chapman, E. Liu, and X. Li, “Modelling frequency-dependent seismic anisotropy in fluid-saturated rock with aligned fractures: implication of fracture size estimation from anisotropic measurements,” *Geophys. Pros.*, vol. 51, pp. 381–392, 2003.

- [86] L. Pyrak-Nolte, *Seismic visibility of fractures*. PhD thesis, Berkeley, 1988.
- [87] E. Hardin, C. Cheng, F. Paillet, and J. Mendelson, “Fracture characterisation by means of attenuation and generation of tube waves in fractured crystalline rock at Mirror Lake, New Hampshire,” *J. Geophys. Res.*, vol. 92, pp. 7989–8006, 1987.
- [88] R. Lubbe and M. Worthington, “A field investigation of fracture compliance,” *Geophys. Pros.*, vol. 54, pp. 319–331, 2006.
- [89] M. Schoenberg and C. Sayers, “Seismic anisotropy of fractured rock,” *Geophysics*, vol. 60, pp. 204–211, 1995.
- [90] M. Schoenberg, “Acoustic characterization of underground fractures,” *68th SEG Expanded Abstracts*, 1998.
- [91] E. Liu, J. Hudson, and T. Pointer, “Equivalent medium representation of fractured rock,” *J. Geophys. Res.*, vol. 105, no. B2, pp. 2981–3000, 2000.
- [92] C. Sayers and D. Han, “The effect of pore fluid on the stress-dependent elastic wave velocities in sandstones,” *72nd SEG Expanded Abstracts*, 2002.
- [93] E. Liu, J. Queen, X. Li, M. Chapman, S. Maultzsch, H. Lynn, and E. Chesnokov, “Observation and analysis of frequency-dependent anisotropy from a multicomponent VSP at Bluebell–Altamont field, Utah,” *J. App. Geophys.*, vol. 54, no. 3–4, pp. 319–333, 2003.
- [94] A. Al-Anboori, *Anisotropy, focal mechanisms, and state of stress in an oilfield: passive seismic monitoring in Oman*. PhD thesis, University of Leeds, 2005.
- [95] O. Al-Harrasi, J.-M. Kendall, and M. Chapman, “Fracture characterization using frequency-dependent shear wave anisotropy analysis of microseismic data,” *Geophys. J. Int.*, vol. 185, pp. 1059–1070, 2011.
- [96] M. Chapman, “Frequency-dependent anisotropy due to meso-scale fractures in the presence of equant porosity,” *Geophys. Pros.*, vol. 51, no. 5, pp. 369–379, 2003.
- [97] L. Pyrak-Nolte and D. Nolte, “Frequency dependence of fracture stiffness,” *Geophys. Res. Lett.*, vol. 19, no. 3, pp. 325–328, 1992.
- [98] A. Baird, J.-M. Kendall, and D. Angus, “Frequency dependent seismic anisotropy due to fracture: Fluid flow versus scattering,” *Geophysics*, vol. 78, no. 2, pp. WA111–WA122, 2013.
- [99] J. Hudson, “A higher order approximation to the wave propagation constants for a cracked solid,” *Geophys. J. R. astr. Soc.*, vol. 87, pp. 265–274, 1986.

- [100] L. Thomsen, “Elastic–anisotropy due to aligned cracks in porous rock,” *Geophys. Pros.*, vol. 43, no. 6, pp. 805–829, 1995.
- [101] J.-M. Kendall, Q. Fisher, S. C. Crump, J. Maddock, A. Carter, S. Hall, J. Wookey, S. Valcke, M. Casey, G. Lloyd, and W. B. Ismail, “Seismic anisotropy as an indicator of reservoir quality in siliclastic rocks,” in *Structurally Complex Reservoirs* (S. Jolley, D. Barr, J. Walsh, and R. Knipe, eds.), vol. 292, pp. 123–136, Geological Society of London, Special Publications, 2007.
- [102] R. Brown and J. Korringa, “On the dependence of the elastic properties of a porous rock on the compressibility of the pore fluid,” *Geophysics*, vol. 40, pp. 608–616, 1975.
- [103] L. Thomsen, “Weak elastic anisotropy,” *Geophysics*, vol. 51, no. 10, pp. 1954–1966, 1986.
- [104] J. Tromp, “Dawn of a new era in computational global seismology,” *Seis. Res. Lett.*, vol. 72, no. 6, pp. 639–640, 2001.
- [105] D. Komatitsch, C. Barnes, and J. Tromp, “Simulation of anisotropic wave propagation based upon a spectral element method,” *Geophysics*, vol. 65, no. 4, pp. 1251–1260, 2000.
- [106] Q. Liu and Y. Gu, “Seismic imaging: From classical to adjoint tomography,” *Tectonophysics*, vol. 566–567, pp. 31–66, 2012.
- [107] R. Pratt, “Velocity models from frequency–domain waveform tomography: past, present and future,” in *EAGE 66th Conference & Exhibition*, (Paris, France), EAGE, June 2004.
- [108] C. Shin, D.-J. Min, K. Marfurt, H. Lim, D. Yang, Y. Cha, S. Ko, K. Yoon, T. Ha, and S. Hong, “Traveltime and amplitude calculations using the damped wave solution,” *Geophysics*, vol. 67, no. 5, pp. 1637–1647, 2002.